This is to certify that the

thesis entitled

THE USE OF RAMAN AND FLUORESCENCE SPECTROSCOPY TO STUDY CRYSTALLIZATION IN SITU

presented by

Robert John Richards

has been accepted towards fulfillment
of the requirements for

Master of Science degree in Chemical Engineering

Major professor

Date July 26, 1990

THE USE OF RAMAN AND FLUORESCENCE SPECTROSCOPY TO STUDY CRYSTALLIZATION *IN SITU*

By

Robert John Richards

A THESIS

Submitted to
Michigan State University
in partial fulfillment of the requirements
for the degree of

MASTER OF SCIENCE

Department of Chemical Engineering

1996

ABSTRACT

THE USE OF RAMAN AND FLUORESCENCE SPECTROSCOPY TO STUDY CRYSTALLIZATION *IN SITU*

By

Robert John Richards

Crystallization is the oldest separation and purification process known to man. It can be used for a wide range of processes. Much of the basic research in crystllization centers on understanding factors which affect crystal size distribution (CSD), bulk density, filterability, slurry viscosity, and dry solids flow properties. These properties in turn depend on CSD and crystal morphology. The factors which affect the fore-mentioned properties are also wide and varied, and often require a great deal of trial and error to obtain parameter information needed to produce the desired product.

To improve production, it would be beneficial to develop tecniques that measure crystallization parameters quickly and efficiently, without trial and error. Ideally, these methods could be done *in situ*, thus minimizing disruptions to the system. Spectroscopic methods offer a means to determine crystallization conditions, with the goal being to improve the process, and ultimately develop a system for on-line control.

In this work, fluorescence and Raman spectroscopy are investigated as means to determine crystallization parameters. Fluorescence spectroscopy is used to detect solution changes in aqueous sugar systems, with emphasis on sensitivity in the supersaturated region. Raman spectroscopy is used to observe a solvent-mediated phase transformation from both the solution and the solid sides of the system.

ACKNOWLEDGEMENTS

I give my professional acknowledgements to Kris Berglund, Tom Carter, Beátrice Torgerson, Laurie Tanner, and Robert Buxbaum. I also wish to thank LEK pharmaceuticals, Ljubljana, Slovenia for the cimetidine.

Funding was provided by the National Needs Fellowship Program and the Cooperative State Research Service of the United States Department of Agriculture, Grant Number 90-34189-5014. Additional Support was provided by the Crop and Food Bioprocessing Center/Research Excellence Fund at Michigan State.

I thank everyone who accepts and respects me for who I am. Their understanding has allowed me to make it this far.

TABLE OF CONTENTS

TABLE OF CONTENTS (Continued)

CHAPTER PAGE

LIST OF TABLES

LIST OF FIGURES

LIST OF FIGURES (Continued)

FIGURE PAGE

LIST OF FIGURES (Continued)

FIGURE PAGE

LIST OF SYMBOLS

A_k = the preexponential constant

E = the electric field vector of incident light

e = the exponential function

K_θ = the propagation direction

m = the dipole moment vector

Q_k = the set of normal coordinates

t = time

α = the polarizability tensor

Φ_n = the direction-cosine matrix

ν_θ = the monochromatic wave frequency

Chapter 1

Background

1.1: Introduction

Crystallization is the oldest unit operation in chemical engineering. The first known application was the separation of sodium chloride from sea water during biblical times. Almost every chemical industry employs crystallization as a separation or purification step during production. Crystallization's primary purpose is to separate a pure product from an impure mixture, but often additional criteria such as crystal size distribution, bulk density, and filterablility also need to be met. These properties are dependent upon path, thus system changes directly affect the final product. System parameters have been, and are still usually determined through trial and error, causing the optimization of a production process to be laborious and time consuming. Crystallization has often been thought of as an art form rather than a science due to these methods of improvement.

Attempts to characterize crystallization were first done in the early 1960's when Mullin[1] published the first work that treated crystallization phenomena in a general sense, rather than treating each system separately. Another important publication was Randolph and Larson's[2] "Theory of Particulate Processes" which gave a mathematical interpretation of the population balance, allowing for prediction of crystal size distributions in realistic industrial crystallizers. These two books discussed the effects of solution characteristics and phase equilibria on crystallization, pointing out the need for analysis techniques that can accurately determine these properties.

In order to achieve crystals with desired characteristics, system parameters that affect the fore-mentioned criteria must be determined to allow for appropriate control. The

use of several analysis techniques to look at crystallization from both the solution and solid sides of the system have been developed to aid in this. Randolph and Larson pioneered two methods, one being the use of a Coulter particle counter to determine crystal size distributions and the other the use of a mixed suspension, mixed product removal (MSMPR) crystallizer. Myerson and coworkers3 have looked at concentrated solutions of both electrolytes and non-electrolytes using diffusion and viscosity measurements. Narayanan and Youngquist[4] have attempted to use electrical conductivity to determine solution properties in several inorganic salt systems.

The use of spectroscopic techniques in the field of crystallization has received much attention in recent years due to their ability to observe systems *in situ*. When a system can be monitored *in situ*, disturbances can be minimized, reducing experimental error and allowing for better control. Richardson *et. al.*[5] used NMR to determine water mobility in aqueous sucrose solutions. Mathlouthi[6] undertook x-ray diffraction studies to investigate molecular association in aqueous sugar solutions.

Raman and fluorescence spectroscopy are two techniques which offer promise as analytical tools to monitor crystallization *in situ*. Previous work has shown that both methods have potential in this area. Cerreta and Berglund[7] showed that the Raman spectroscopy could be applied to the aqueous glucose system for observation of conditions from both the solid and solution sides of the system, with glucose solutions, anhydrous glucose, and glucose monohydrate exhibiting unique spectra in the fingerprint region. Chakraborty and Berglund[8] have demonstrated that pyranine could be used as a trace fluorescent probe to study the structure of aqueous sugar solutions.

This study further explores the potential of fluorescence and Raman spectroscopy to determine crystallization parameters. In specialty chemical production, it is advantageous to use *in situ* analysis techniques for on line control since high purity standards are required. *In situ* monitorization greatly reduces or eliminates system disturbances caused by on-line sampling while providing more accurate real time data. In the making of

pharmaceuticals, four nines (99.99 %) purity and batch to batch consistency are necessary criteria to meet FDA standards, thus good control of system parameters is needed to meet these demands. Raman spectroscopy's ability to observe conditions of both the solid and solution sides of a system makes it ideal to study parameters in the crystallization of pharmaceuticals. Along with this, crystal polymorphism can be observed since different crystalline phases have different Raman spectra.

Trace fluorescent spectroscopy has proven to be a viable method to observe conditions in supersaturated solutions. Pyranine is a valuable probe to study aqueous sugar solutions, but it is not accepted by the FDA for use in foods. This incompatibility with food doesn't allow pyranine to be used as an on-line trace fluorescent probe, thus its potential for industry is confined to non-food applications. Carminic acid, an F,D and C approved dye was chosen as a possible replacement since many of the same qualities of pyranine, but it is safe for use in food and drugs.[9]

1.2: Overview of Crystal Polymorphism

Crystal Polymorphism is the ability of a chemical compound to exist in more than one crystalline form.[10] Different structures are called polymorphs or polymorphic modifications. The ability of a solid to crystallize into more than one crystalline phase depends on several conditions that exist during crystallization. Temperature, pressure, and solvent are all parameters that can affect the polymorph obtained.

Polymorphs have similar chemical properties but dissimilar physical properties. For example calcium carbonate can exist in two forms, calcite and aragonite. Both forms have the same chemical properties, but exhibit different physical properties. Calcite is a rhombohedral uniaxial crystal with a density of 2.71 gm/cc whereas aragonite exists as an orthorhombic biaxial crystal with a density of 2.94 gm/cc.

The importance of studying polymorphic phenomena in pharmaceutical compounds lies in the different physical properties between polymorphs.[11] Differences in crystal form

can cause differences solubility, which in turn causes differences in bioavailability and drug effectiveness. Tableting characteristics are also affected depending on the polymorph being processed.[12,13] These types of discrepancies are simply unacceptable to the Food and Drug Administration, thus it is very important to understand crystallization parameters that affect polymorphism.

A particular area of polymorphism that causes problems in the pharmaceutical industry is that of unwanted phase transitions.[14,15,16] Often times the desired phase produced is the metastable phase which under certain conditions can transform to the stable phase. A phase transition such as this will reduce the solubility and bioavailability of the drug, making it less effective. In other cases the stable phase may be preferred, but it can be difficult to make large amounts of it due to kinetic factors. For a situation such as this, it is often advantageous to make the metastable phase and then set the conditions to force a phase transformation to the stable phase.

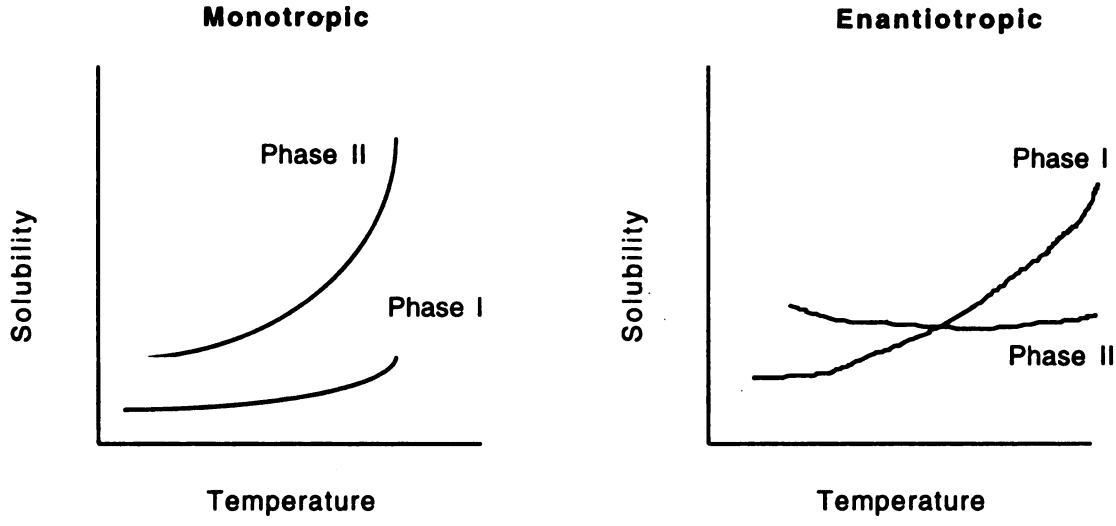

Figure 1 : Idealized curves of monotropic and enantiotropic systems

There are two types of polymorphic systems, enantiotropic and monotropic. An enantiotropic system has an interconversion temperature below the melting point of each polymorph whereas a monotropic system doesn't. A monotropic system has one polymorph that is the stable form throughout the temperature range. Figure 1 shows

idealized monotropic and enantiotropic systems. For monotropic systems, the stable phase exhibits lower solubility throughout the temperature range.

There are two ways that a phase transformation can take place. In the first the metastable phase can undergo an internal rearrangement of molecules or atoms that occurs

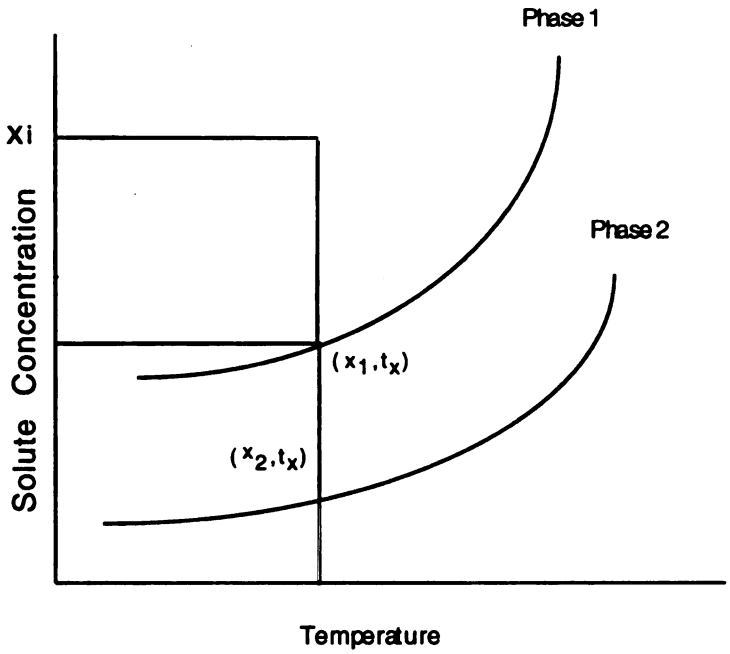

Figure 2: Schematic of a solventmediated phase transition

in the solid state.[17] The second route is aided by the presence of a solvent in contact with the metastable phase which allows it to dissolve and allows the growth and nucleation of the stable phase independently. This type of phase transformation is called a solvent-mediated phase transformation.[18]

The changes in solute concentration as a solvent-mediated phase transformation takes place can be explained in the following way. A solution at composition x_i is supersaturated with respect to both phase I and phase II. Figure 2 gives a schematic of this. As nucleation and growth occurs, the majority of the crystals will be the metastable phase, with a few of the crystals being that of phase II, following Ostwald's law of stages.[19]

During the initial growth phase the solute concentration will fall from x_i to x_1. This being the case, it is now possible for the phase transformation to take place via solvent-mediation since there is a slurry of metastable and stable phase crystals in contact with a solution saturated with respect to phase I and supersaturated with respect to phase II. As the phase transformation takes place, phase II grows at the expense of the dissolution of phase I, thus the solute concentration remains constant as this occurs. Once all of phase I is dissolved, phase II will continue to grow until the solution reaches the solution composition at x_2, which is the saturation composition of phase II.

Figure 3 shows the changes in supersaturation with respect to time as the phase transformation takes place. The s_{12} point represents the initial supersaturation at the beginning of the phase transformation where the solute concentration is x_1. Region 1 of the curve is the initial onset of the phase transformation where the growth of phase two is faster than the dissolution of phase one.

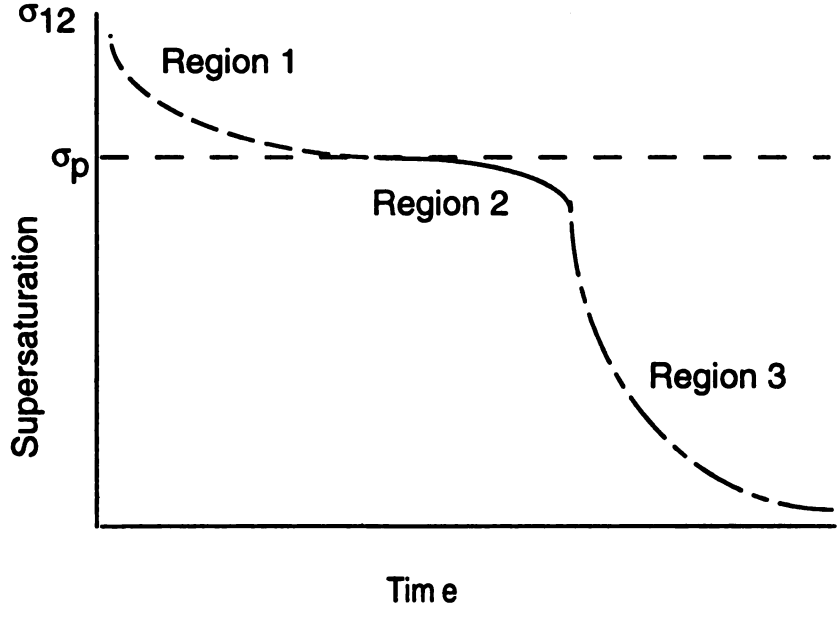

Figure 3: Idealized Changes in Supersaturation During a Solvent-Mediated Phase Transformation.

As the transformation proceeds, region 2 represents a region of approximately constant supersaturation, where the dissolution rate of phase I equals the growth rate of

phase II. Region 3 represents the time domain where the phase transformation is complete, and where only phase II is growing.

1.3: Common Analytical Techniques Used to Study Crystal Polymorphism

There are several methods by which to characterize polymorphic systems. Methods include X-ray techniques, FT-IR, thermal techniques, solubility measurements and hot stage microscopy[20-23].

X-ray crystallography is the most common way to determine molecular information of a crystalline solid. The method is an excellent way to determine the lattice structure of crystals and can also be used to obtain the packing relationship of molecules in a solid. X-ray crystallography is not practical to use with a mixture of crystals or crystals that are small in size, since the technique requires one large crystal for analysis.

FT-IR spectroscopy is extremely sensitive to both structure and conformation, and is very good to investigate the solid state. There are several examples in literature that show that FT-IR spectral differences can be used to distinguish different polymorphs. It is difficult to use FT-IR in solvent-solute systems because the solvent spectra is usually much stronger than the solute spectra, especially when the solubility is low. Another drawback is that FT-IR cannot look at the far-IR region of the spectrum due to instrumentation limitations, thus the lattice vibration region of the spectrum cannot be observed by FT-IR.

Thermal techniques such as Differential Scanning Calorimetry (DSC) and Thermal Gravimetric Analysis (TGA) are used to determine melting points and to detect the presence of solvates. These techniques lack resolution, which causes problems with polymorphs of similar melting points. It is also difficult to differentiate between solid-solid transformations and recrystallization processes. When done in conjunction with hot stage microscopy, DSC endotherms and exotherms can be correlated with either solid-solid phase transitions or solid-liquid phase transitions.

Since polymorphs exhibit different solubilities, dissolution and/or solubility measurements are often used to distinguish between two or more crystal forms. These studies are especially important when done on pharmaceutical products since solubility differences result in bioavailability differences.

1.4: General Theory of Raman Spectroscopy

Light scattering can occur when light interacts with matter. When the scattering is elastic and of the same frequency as that of the incident radiation, it is known as Rayleigh scattering. The other type is inelastic and can be further broken up into two types of light scattering: scattering of longer wavelength light which is known as Stokes Raman scattering and scattering of shorter wavelength which is known as anti-Stokes Raman scattering.[24]

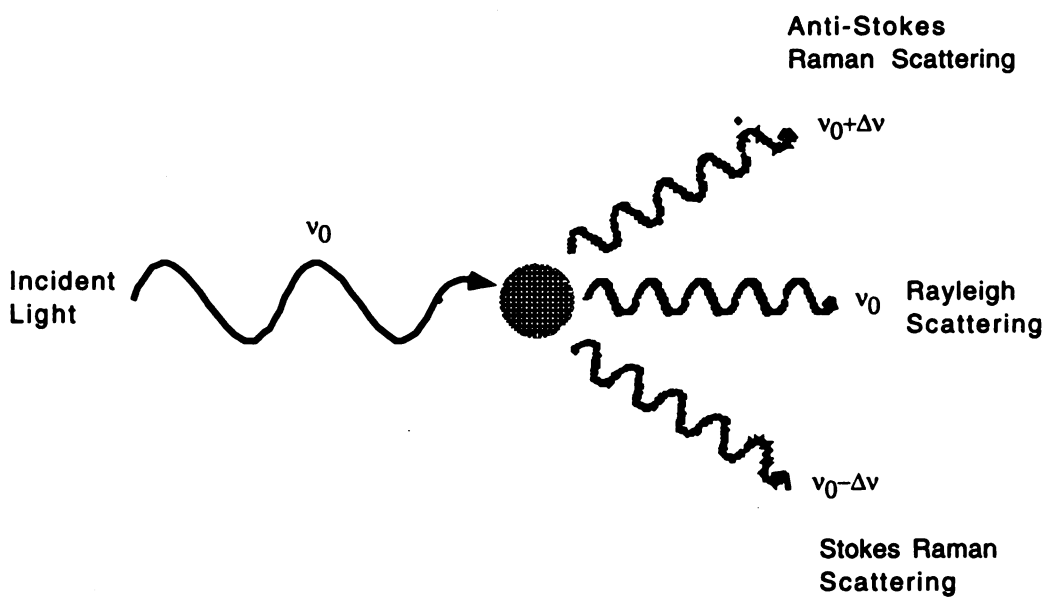

Figure 4: Schematic of Rayleigh, Stokes Raman, and Anti-Stokes Raman Scattering

Raman scattering is the result of light interacting with the electrons in a molecule. There are two types of Raman scattering. Resonance Raman scattering occurs when the incident frequency is near the electronic absorption band of the molecule, resulting in a

coupling of electronic and vibrational transitions. Non-resonance or spontaneous Raman scattering occurs when the energy of the incident light is not sufficient to raise the molecular electrons to a higher electronic state.

The frequency of Raman scattering is independent of the excitation wavelength, but the intensity is directly proportional to v^4. This means that regardless of the excitation wavelength, the Raman spectrum will show the same shift in cm^{-1}, but the spectrum will be more intense as the excitation wavelength is decreased. Ideally it seems that the excitation wavelength should be kept as low as possible, but it is quite common to encounter problems with fluorescence as excitation wavelength is decreased.[25]

Interference from fluorescence can pose a problem since it is much more intense than Raman scattering. The intensity of Raman spectra compared to that of fluorescence spectra is often 10^{-3} lower than that of fluorescence intensity. This can be a problem for many compounds such as specialty chemicals and pharmaceuticals, which often will fluoresce when excited with UV, blue, or green light. To avoid this difficulty, Raman spectroscopy of pharmaceutical compounds is done using visible red or IR as the excitation source.[26]

1.5: Low Frequency Raman Spectra of Crystals

Based on the theoretical work done by Turrell[27], Raman spectral differences in the low frequency region of the spectrum can depend on several factors. Crystal class, molecular orientation, bond length, and force constants can all affect the spectra seen at low frequencies. It is possible for a compound to exist in two crystalline phases which are of the same crystal system, but the crystal class, molecular orientation, bond length and force constants among molecules are different. This accounts for Raman spectral differences in lattice vibrations. Since a polymorphic substance by definition can exist in more than one crystalline state, different polymorphs should exhibit Raman spectral differences in the

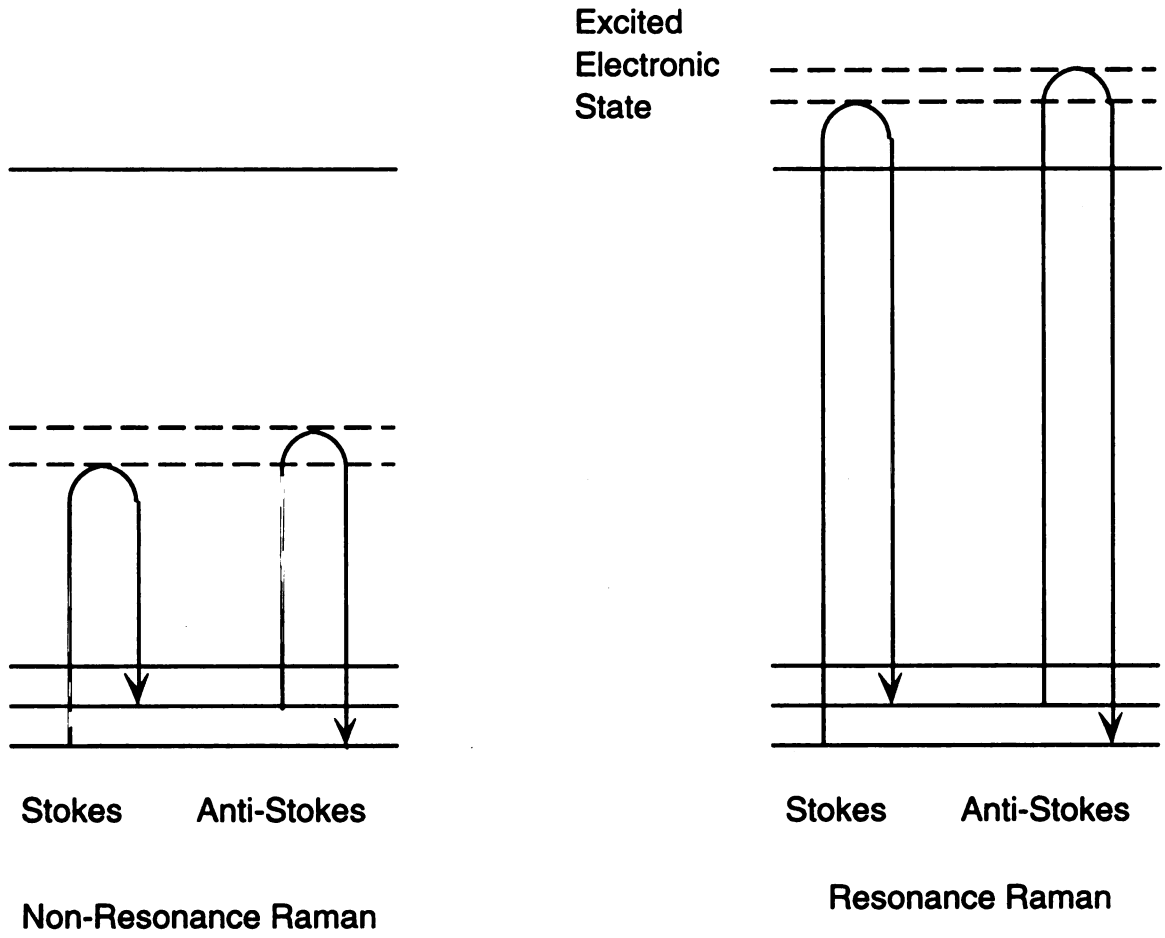

Figure 5: Contrast Between Resonance and Non-Resonance Raman Scattering

lattice vibration region, even if they don't show Raman spectral differences in the fingerprint region.

Raman spectra of crystals in the lattice vibration region has been used for several decades to observe polymorphic changes of crystal structure in the solid state.[25] These experiments involved the observation of spectral changes in a large single crystal irradiated at known orientations. Up until now, solvent-mediated phase transformations have not been investigated with Raman spectra in the lattice vibration region.

When a molecule interacts with monochromatic light, there are two oppositely directed forces that act on the electrons and the nuclei, respectively. Due to this, the nuclei and electrons will be displaced relative to each other, causing an induced dipole moment. This can be expressed as

$$m = \alpha E \qquad (1)$$

where m is the dipole moment vector, α is the polarizability tensor, and E is the electric field vector of the incident light. Equation (1) can also be used to describe the induced dipole moment in a crystal when it interacts with light.

E represented as a function of time is

$$E = E^{o} e^{-2\pi(K_e \cdot r - \nu_e t)} \qquad (2)$$

where ν_e is the monochromatic wave frequency, K_e is the propagation direction, and t is time. The actual occurrence of Raman scattering depends on the polarizability tensor, which in turn depends on the instantaneous position of atoms in the lattice. If α is a function of the set of normal coordinates Q_k, it can be expressed as

$$\alpha = \alpha_o + \sum_k^n \left(\frac{\partial \alpha}{\partial Q_k}\right)_o Q_k + \frac{1}{2} \sum_{k,k'}^{n,n'} \left(\frac{\partial^2 \alpha}{\partial Q_k \partial Q_{k'}}\right) Q_k Q_{k'} + \ldots \quad (3)$$

Generally, only first order (single photon) scattering is considering, thus the polarizability tensor can be approximated as

$$\alpha = \alpha_o + \sum_k^n \left(\frac{\partial \alpha}{\partial Q_k}\right)_o Q_k \quad (4)$$

Since the lattice waves can be represented by

$$Q_k = A_k e^{\pm 2\pi i (k_k \bullet r - \nu_k t)} \quad (5)$$

Equation (1) can be expressed as: (6)

$$m = \alpha_o E^\circ e^{-2\pi i (K_e \bullet r - \nu_e t)} + \sum_k \left(\frac{\partial \alpha}{\partial Q_k}\right)_o A_k E^\circ e^{2\pi i [(K_e \pm k_k) \bullet r - (\nu_e \mp \nu_k) t]}$$

The first term in equation (5) represents Rayleigh scattering.If in equation (6) $\frac{\partial \alpha}{\partial Q_k} \neq 0$,then Raman scattering occurs. For a free molecule, $\frac{\partial \alpha}{\partial Q_k}$ or α'can be represented in tensor form as a matrix:

$$\frac{\partial \alpha}{\partial Q_k} \equiv \alpha'^k = \begin{matrix} \alpha_{xx}'^{(k)} & \alpha_{xy}'^{(k)} & \alpha_{xz}'^{(k)} \\ \alpha_{yx}'^{(k)} & \alpha_{yy}'^{(k)} & \alpha_{yz}'^{(k)} \\ \alpha_{zx}'^{(k)} & \alpha_{zy}'^{(k)} & \alpha_{zz}'^{(k)} \end{matrix} \quad (7)$$

The orientations of each molecule in a crystal lattice can also be represented in tensor form:

$$\Phi_n = \begin{matrix} a_x & a_y & a_z \\ b_x & b_y & b_z \\ c_x & c_y & c_z \end{matrix} \tag{8}$$

To account for more than one molecule in a given crystal lattice, the respective polarizability tensors must be transformed into crystal fixed coordinates. This can be done as follows.

$$\alpha_n{}'^{(k)} = \Phi_n \, \alpha'^{(k)} \, \Phi_n{}^{T} \tag{9}$$

If additivity of polarizabilities is assumed, the unit cell polarizability written as a function of molecular coordinates becomes.

$$\alpha = \sum_k [\sum_n \alpha_n{}'^{(k)} \, Q_{k,n}] \tag{10}$$

Using factor group analysis, the molecular normal coordinates can be combined by using the unit cell symmetry. The general case for this gives:

$$Q_k{}^{(i)} = \sum_n Q_{k,n} \tag{11}$$

where i represents A_g, B_g, A_u, B_u, etc., and n represents the number of molecules in the unit cell. The signs of $Q_{k,n}$ depend on the orientation of the molecules in the unit cell. By

substituting the inverse of (10) into (9) , an expression for the polarizability of the unit cell can be obtained.

$$\alpha_k^{(i)} = \sum_k [(\sum_n \Phi_n \alpha_k \Phi_n^T) Q_k^{(i)} \qquad (12)$$

The derivative of equation (12) will give the tensor necessary to determine the fundamentals of crystal lattice vibrations for a given system.

$$\alpha_k'^{(i)} \equiv \frac{\partial \alpha_k^{(i)}}{\partial Q_k^{(i)}} = \sum_k [(\sum_n \Phi_n \alpha_k \Phi_n^T) \qquad (13)$$

Depending on the crystal system, the form of equation (12) will be different. The mathematics outlined above can be carried out rigorously for the system under study, or tabulated results of the tensor forms can be found in literature[28] for each of the seven crystal systems. This gives a general method by which to predict the number of fundamental lattice vibrations, but it doesn't predict the frequencies of these vibrations, nor does it account for combinations and overtones.

1.6. Theory of Emission Spectroscopy

Fluorescence and phosphorescence are processes in which radiation is emitted by molecules that have been excited by the absorption of radiation. Fluorescence and phosphorescence can be distinguished by the multiplicities from which each respective molecule emits radiation. If the states from which the emission originates and terminates have the same multiplicity, then fluorescence occurs. Fluorescence usually occurs between the lowest S_1 vibrational level and the S_0 states, although molecules excited to a higher singlet state can exhibit fluorescence. If the states are different in spin, then phosphorescence occurs. The most common phosphorescence occurs between the T_1 state

and the S_0 state. A practical way to distinguish between the two processes would be to determine excited state lifetimes, since the fluorescence lifetimes are several orders of magnitude shorter than phosphorescence lifetimes[29].

Radiationless processes are caused by the conversion of electronic energy to vibrational energy. When this occurs between the lowest singlet state (S_1) and the lowest triplet state (T_1) it is referred to as inter-system crossing. All other cases are known as internal conversion, which results in no light being emitted.

Light can be represented in terms of energy by Planck's equation, $E=h\nu$, thus absorption and emission can be thought of as an energy absorption and emission process. When light impinges on matter, two things can happen: it can pass through the matter with no absorption or it can be absorbed by the molecules causing them to go from a lower energy state to a higher energy state. In a sense, the absorption and emission process could be looked at as an energy cycle with the same beginning and end points, where energy is neither created or destroyed, but is converted to either radiative or non-radiative processes. Radiative processes are those in which the excited molecule falls from a higher energy level to a lower energy level and emits light, whereas non-radiative processes are those in which the excited molecule falls to from a higher energy level to a lower energy or vibrational level without emitting light. For gases and crystals, it is possible that the absorption and emission energies can be the same, thus the excitation wavelength and emission wavelengths are also the same. This process is known as resonance radiation. For solutions, the emission energy is lower due to solvent interactions. Lower emission energy results in a spectrum of longer wavelength. This process is known as Stokes fluorescence.[30]

Each fluorescent molecule has two characteristic spectra: the excitation spectrum and the emission spectrum. The shape of the excitation spectrum is identical to the absorption spectrum, and it is independent of the emission wavelength at which it is measured.[31,32] The emission spectrum is usually a mirror image of the excitation

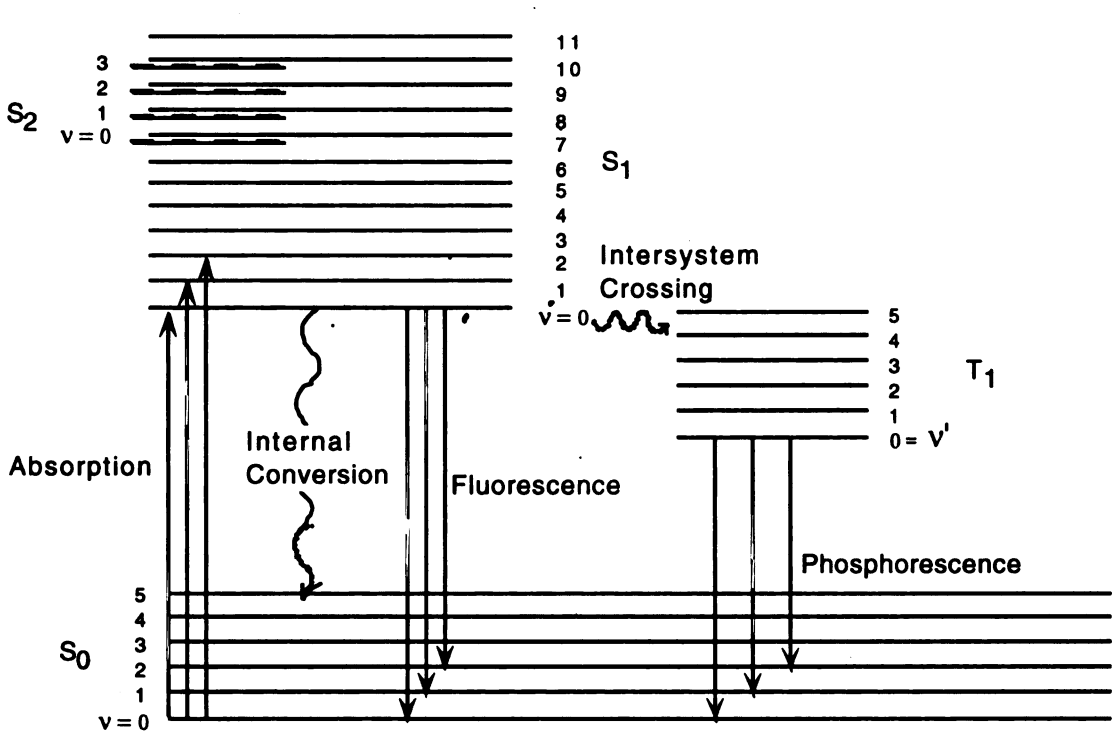

Figure 6: Schematic of light absorption and emission

spectrum, and is independent of excitation wavelength. This wavelength independence doesn't mean that the emission intensity will also be independent of excitation wavelength, since the intensity depends on factors such as the relative strength of absorption and non-radiative contributions.

1.7 Instrumentation and Applications of Emission Spectroscopy

The measurement of fluorescence requires a light source, excitation and emission filters, detector, amplifier, and a readout device (usually a computer). The light source is preferentially filtered at the excitation stage so that the sample can be excited by a monochromatic beam of light. The emission signal wavelength is measured by the placing the emission filter between the sample and the detector usually located at a 90° angle from the incident excitation beam. The detector is amplified and the final signal is sent to a readout device, where the signal intensity can be plotted as a function of emission wavelength.

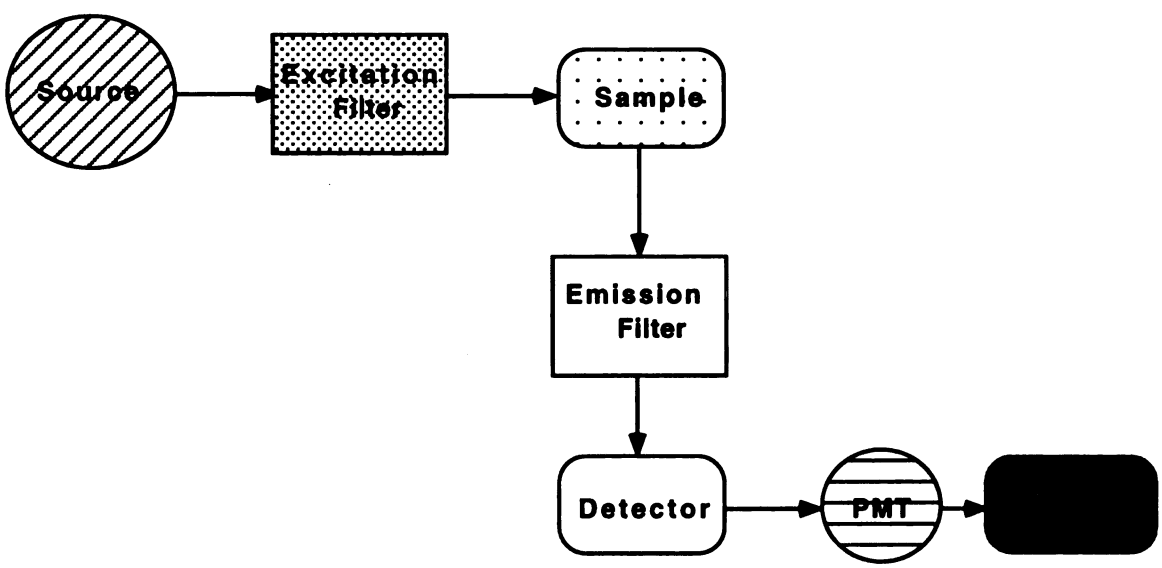

Figure 7: Block Diagram of Typical Emission Spectroscopy Instrumentation

The use of emission spectroscopy as an analytical tool offers several advantages,

namely extreme sensitivity, excellent specificity and dependence on environmental factors such as temperature, viscosity, and pH. Quantitative methods of fluorimetry can be broken up into two branches: The intrinsic fluorescence of a material can be measured as a function system conditions or a fluorescent probe can be added as an extrinsic monitor of system conditions in an amount that will have little or no effect on the system. Since the majority of compounds do not fluoresce, it is often advantageous to use the method of a trace fluorescent probe. Since fluorescent techniques have high quantum efficiencies, it is possible to use small quantities ($< 10^{-3}$) that have little or no effect on system conditions. Trace fluorescent probes can be used in a qualitative fashion to detect the presence or absence of a reagent. Staining techniques make use of a fluorescent additive to determine various cell components. Fluorochromes can be used *in vivo* to define the structures involved in the production of hydrolytic enzymes and to determine enzymatic activity. Fluorescent-labelled specific antibodies detect visually specific proteins in foods. Nanogram quantities of metal and metalloid ions in solution will complex to various additives allowing for quantitative concentration measurements by correlating the fluorescence intensity of the complex to ion concentration.

Fluorescence spectroscopy can be applied to crystallization by adding trace amounts of fluorophore to a system to look at the solution conditions. Both steady state and time-resolved fluorescence spectroscopy have recently been used. Chakraborty and Berglund[10] used the steady-state fluorescence spectra of Pan[33] *et al.* showed that fluorescence lifetimes and rotational correlation times of pyranine and pyrene butyric acid in aqueous sucrose solutions indicated the formation of a network of hydrogen bonding interactions between sucrose molecules. He further used pyranine in supersaturated protein solutions to measure anisotropy and correlate these measurements with optimal crystallization conditions.

References

1. J. W. Mullin, Crystallization, (Butterworth and Company, London 1961), preface.

2. A. D. Randolph and M. A. Larson, Theory of Particulate Processes, (Academic Press, Inc. 1971) chapter 3.

3. A. S. Meyerson and K. Toyokura, Crystallization as a Separations Process, (American Chemical Society, 1990) chapter 1.

4. H. Narayanan and G. R. Youngquist, *AICHE Symposium Series*, **253**, (1987) 1.

5. S. J. Richardson and M. P. Steinberg, Journal of Food Science, **52**, (1987) 806.

6. M. Mathlouthi et. al., Carbohydrate Research **81**, (1980) 213.

7. M. K. Cerreta and K. A. Berglund, *Journal of Crystal Growth*, **102**, (1990) 869.

8. R. Chakraborty and K. A. Berglund, *Journal of Crystal Growth*, **125**, (1992) 81.

9. The Merck Index, eleventh edition, (Merck and Company, Inc. 1983) pp. 256.

10. Polymorphism and Polytypism in Crystals, A.R. Verma and P. Krishna, (Russian press, 1967) pp. 8-9.

11. Solid State Chemistry of Drugs, S. R. Byrn, (Academic Press, New York, 1982) pp. 29-58, 79-102.

12 M. D. Tudalhar, J. E. Carless, and M. P. Summer, *Journal of Pharmaceuticals and Pharmacology* , **35**, 269-274 (1983).

13. G. A. Ghan, and J. K. Lalla, *Journal of Pharmaceuticals and Pharmacology* , **44**, (1992) 678.

14. R. J. Davey and J .Richards, *Journal of Crystal Growth* , **71**, (1985) 597.

15. K. Matsuda et. al. *Journal of Pharmaceutical Science* , **73**, (1984) 173.

16. R. J. Davey, P. D. Guy, and A. J. Ruddick, *Journal of Colloid and Interface Science*, **108**, (1985) 189.

17. A. I. Kitaigorodsky, et. al. *Journal of Physical Chemistry of Solids* , **26**, (1965) 463.

18. P. T. Cardrew, and R. J. Davey, *Proceedings of the Royal Society of London A*, **398**, (1985) 415.

19. Grundiss der Algemeinen Chemie, W. Ostwald, (W. Engelmann, Leipzig,1899).

20. J. Haleblian, and W. McCrone, *Journal of Pharmaceutical Science*, **58**, (1969) 911.

21. M. Stolz, et. al., *Journal of Pharmaceutical Science*, **78**, (1989) 758.

22. F. A. Chrzanowski et. al., *Journal of Pharmaceutical Science*, **73** (1984) 1448.

23. H. Kamiya, M. Kazuhiro, and K. Morisaka, *International Journal of Pharmaceutics*, **26**, (1985) 197.

24. Raman Spectroscopy in Biology, Principles and Applications, A. T. Tu, (John Wiley and Sons, New York, 1982) pp. 6-14.

25. Raman Spectra of Molecules and Crystals, M.M. Sushchinskii,(Israel Program for Scientific Translations Ltd., New York, 1972) pp. 1-15.

26. Raman Spectroscopy, D. A. Long, (McGraw-Hill, New York, 1977) pp. 1-20.

27. Infrared and Raman Spectra of Crystals, G. Turrell,(Academic Press, New York, 1972) Chapter 5 and 6.

28. Infrared and Raman Selection Rules for Molecular and Lattice Vibrations, W. G. Fateley, et. al.(Wiley Interscience, New York, 1972) Appendix I and II.

29. Fluorescence Analysis in Foods, L. Munck, (Longman Scientific and Technical UK Limited, 1989) Chapter 1 and 2.

30. Practical Fluorescence-Theory, Methods, and Techniques, G. G. Guibault, (Marcel Dekker, New York, 1973) Chapter 1.

31. Theory and Interpretation of Fluorescence, R. S. Bekker, (John Wiley and Sons, New York, 1969) pp. 3.

32. Fluorescence of Solutions, E. S. Bowen, (Longmans, Green and Company,London, 1953) pp. 5.

33. B. Pan et. al., *Journal of Crystal Growth*, **130**, (1993) 587.

Chapter 2

The Use of Raman Spectroscopy to Investigate Solvent Mediated Phase Transformations in Cimetidine

2.1 Introduction

The study of crystal polymorphism is an important aspect of insuring proper consistency in pharmaceutical manufacturing. It is known that different polymorphs exhibit different physical and chemical properties, which in turn cause variances in bioavailability, stability, and tableting characteristics.[1,2]

In the production of pharmaceuticals, crystallization is the method most commonly used to achieve high purity and batch to batch consistency. For a substance that can exist in several different polymorphs, changes in crystallization conditions can change the amount and type of polymorph upon manufacture. Since manufacturing processes are usually operated under non-equilibrium conditions, metastable phases frequently occur. This thermodynamic instability can lead to phase transformations in solution, thus it is important to determine the conditions under which such transformations occur.

Several techniques have been used to characterize polymorphic systems, including, DSC, FT-IR, dissolution studies, and hot-stage microscopy.[1] All of these techniques can be used to distinguish crystalline polymorphs after the fact, but they lack the ability to measure changes *in situ*.

The application of Raman spectroscopy to the analysis of pharmaceutical compounds has become a growing field in the last several years.[3,4] Much of the molecular information that can be obtained from Raman spectroscopy is very similar to that found with FT-IR, but Raman has several key advantages. Raman spectroscopy can be used on samples in the liquid, solid, and gaseous state.[5] In low-solubility systems with water and water-alcohol solvents, the solute spectrum can be seen since these solvents have much

sharper bands that don't interfere with the solute spectrum. The capability to watch system changes *in situ* is another advantage that Raman spectroscopy has over FT-IR since the fore-mentioned solvent transparency allows for detection of solute. Raman spectroscopy also allows for a practical means to obtain low-frequency crystal lattice vibration spectra, which is often important in distinguishing one polymorph from another and can also help determine crystal structure.[6] It is difficult to obtain lattice vibration spectra using mid-infrared instruments since they lack the capability to acquire low frequency or far-IR spectra.

Cimetidine (Figure 1) is a commonly used Gastrointesinal-tract acid secretion inhibitor that exhibits several crystalline polymorphs (A, B, C, and D), all of which have different bioavailabilities.[7] Several crystallization studies have been undertaken to determine conditions which produce each respective polymorph.[8-10] Recently, the solvent-mediated phase transformation of the metastable form A to the stable form B has been studied in isopropanol solutions.[11]

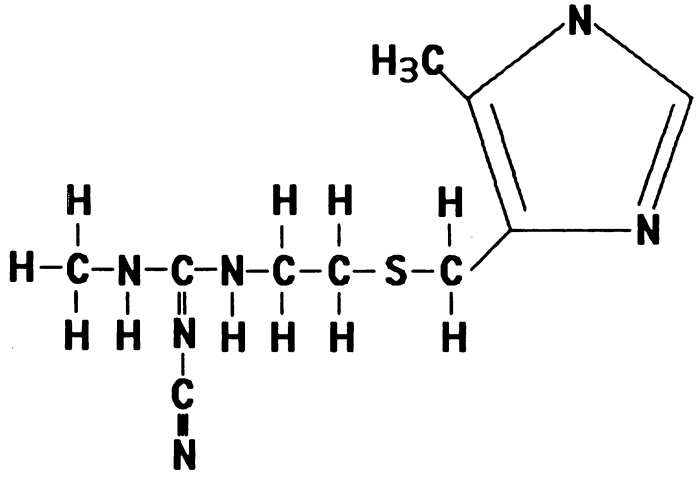

Figure 8: Chemical Structure of Cimetidine.

Work done by Tudor et. al.[12], demonstrated that FT-Raman using IR excitation could be used to distinguish cimetidine polymorphs A, B, and C in the solid state while maintaining effective fluorescence rejection. Their instrumentation, however, did not permit determination of the lattice vibration spectrum. Futhermore, high powers at the sample are required to obtain spectra with acceptable signal to noise ratios due to Raman spectroscopy's inverse wavelength to the fourth power dependence on spectral intensity. In our study, we have used conventional Raman spectroscopy with a Krypton ion laser and a dispersion grating spectrometer to demonstrate the feasibility of the technique and also to answer some new questions about phase transitions in cimetidine-water and cimetidine-water-isopropanol systems, and have investigated the possibility of following these phase transformations *in situ*.

2.2. Procedure

Polymorphs A and B were supplied by LEK Pharmaceuticals in powdered form and were used without further purification. Reagent grade isopropanol (Baker) and HPLC grade water (Sigma) were used for solubility and phase transformation experiments. A schematic of the experimental setup is shown in Figure 4. The processes are outlined in detail below

A Coherent Radiation Innova 90-10 watt constant wave Kr^+ ion laser at 647.12 nm was used as a monochromatic light source for two reasons. First, fluorescence problems were minimized, as the excitation lies away from the absorption of most fluorescing substances. Second, the higher dispersion of red light allowed for easier access to the Raman lattice vibration region without interference from Rayleigh scattering.

The detection system consisted of an EG & G Model 1530-C/Cuv 1024S 256 x 1024 CCD red-enhanced multichannel detector coupled to a Spex 1877 Triplemate triple

monochrometer. Solid samples were analyzed by directing the laser beam through a Zeiss standard microscope that was attached to the Triplemate, whereas liquid samples were analyzed by directing the laser beam through a quartz cuvette mounted before the filter stage. *In situ* spectra of agitated slurries were obtained by directing the laser through a quartz cuvette in a back-scattering sample configuration.

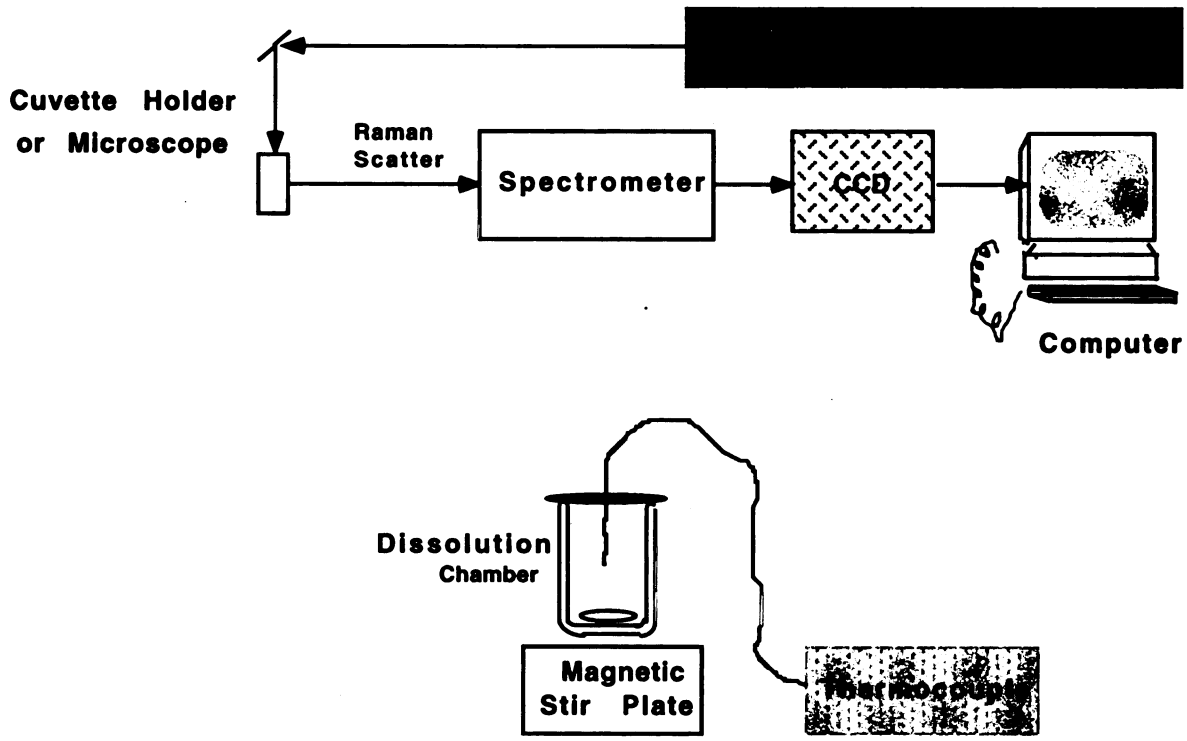

Figure 9: Schematic of experimental setup for cimetidine solubility, phase transformation, and *in situ* studies. The cuvette holder and dissolution chamber were water jacketed for temperature control.

Solutions saturated with respect to phase A were prepared by adding excess A and allowing the mixture to equilibrate in an agitated vessel for 5 hours. Forty-five ml of this saturated solution were filtered and put into a temperature controlled batch crystallizer. Exactly 0.30 g of a known mixture of seed crystals was added. Slurry samples were then drawn off at known time intervals, with the solid and liquid phases being separated through filtration. The spectrum of each phase was recorded in the range of Raman shift 64 to 685

cm^{-1}. Power at the sample for liquid samples was 500 mW and for solid samples was 100 mW. Each spectrum consisted of 30, 10 second scans that were accumulated to improve the signal to noise ratio.

Calibration curves were made by taking spectra of cimetidine/solvent solutions of known composition and plotting the spectral changes versus solute weight percent. The Peak Intensity Ratio (PIR) of a solvent band (494 cm^{-1}) to a solute band (675 cm^{-1}) was used to act as an internal standard, to account for fluctuations in the spectral baselines. Once the calibration curve was made, spectra of the saturated solution of forms A and B were taken and the PIR was compared to that of the calibration curve, thus giving the saturation concentration in weight percent.

2.3. Results and Discussion

The solid state spectra of phase A and phase B in the lattice vibration region are shown in Figure 5. The spectra show distinct differences from 100 to 200 cm^{-1}, 300 to 350 cm^{-1}, 500 to 525 cm^{-1}, and 600 to 650 cm^{-1}.

Typical Raman spectra of cimetidine in isopropanol and/or isopropanol-water solutions are shown in Figure 6. Three distinct isopropanol lines are seen at 494 cm^{-1}, 425 cm^{-1}, and 375 cm^{-1} along with cimetidine spectral lines at 675 and 620 cm^{-1}. Raman scattering from water was insignificant in this region of the spectrum, but a strong Rayleigh tail, typical of Raman spectra of solutions is seen.[16]

The solubility curves (Figure 12 and Figure 13) show that cimetidine can be detected down to levels of 0.5 weight percent in both isopropanol and water. Results similar to the work of Sudo et. al[8] show that Raman spectroscopy is comparable to common methods in determining solubility curves.

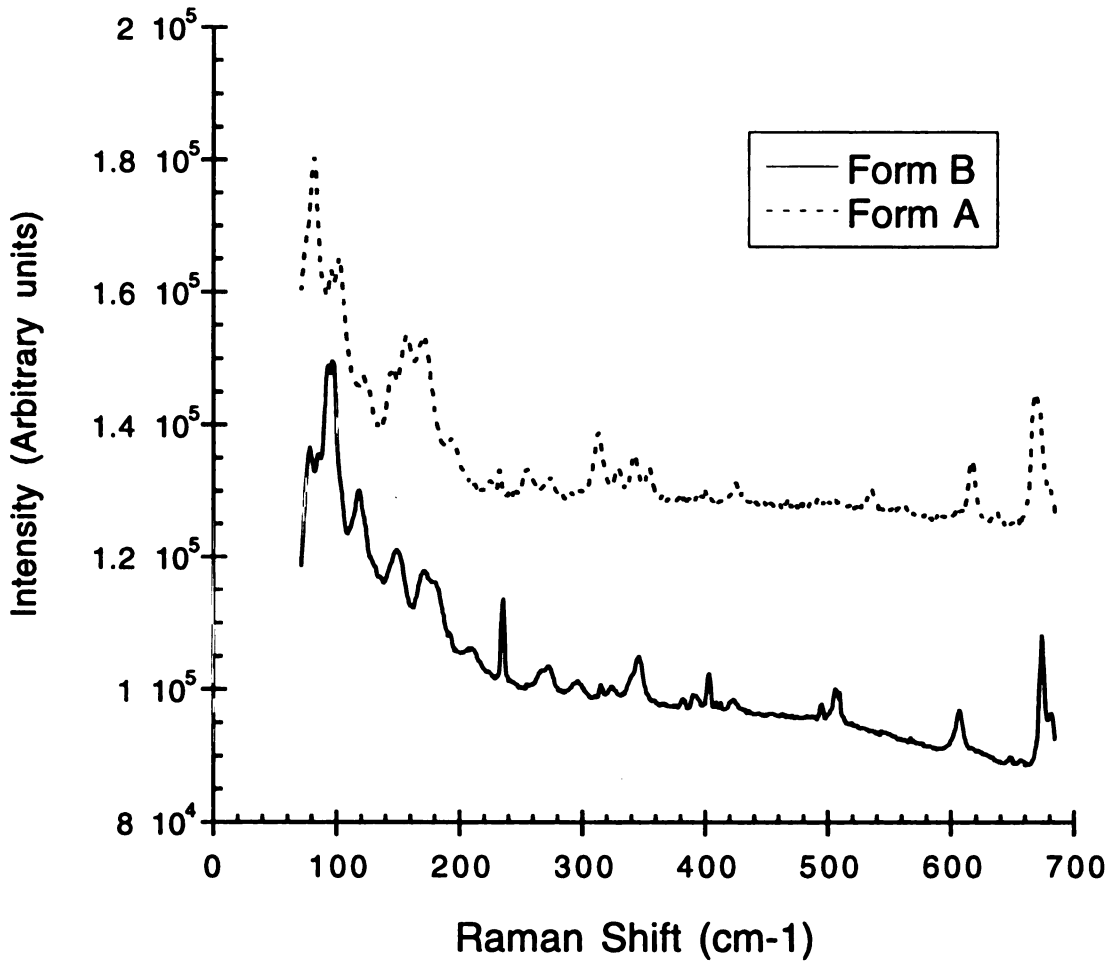

Figure 10: Raman spectra of crystalline cimetidine. Excitation wavelength 647.12 nm, Temperature 25 °C

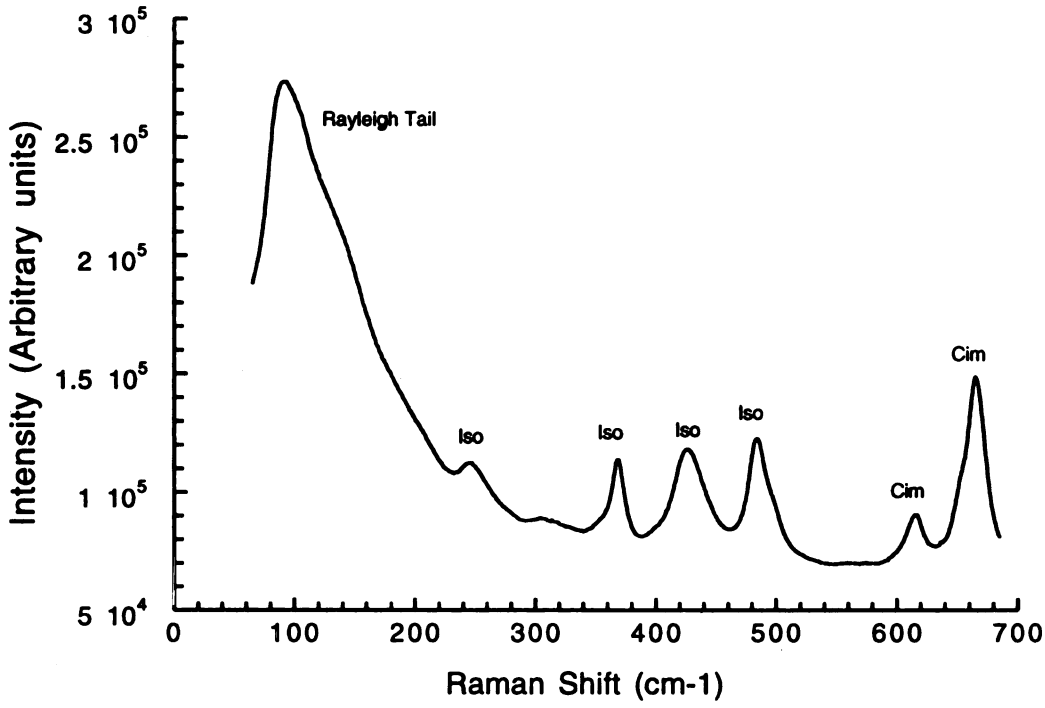

Figure 11: Typical Raman spectra of cimetidine in isopropanol. Excitation wavelength 647.12 nm, Temperature 25 °C

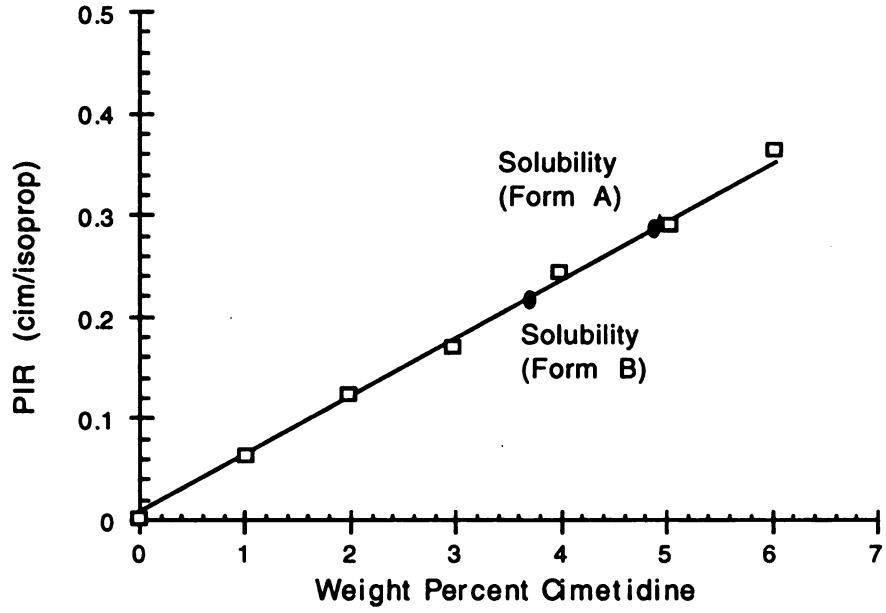

Figure 12: PIR's of 675 cm-1 (cim) to 494 cm-1 (isoprop) as a function of cimetidine concentration in isopropanol solutions. Solubilities are represented by ovals and calibration curve points are represented by squares. Excitation wavelength 647.12 nm, Temperature 50 °C.

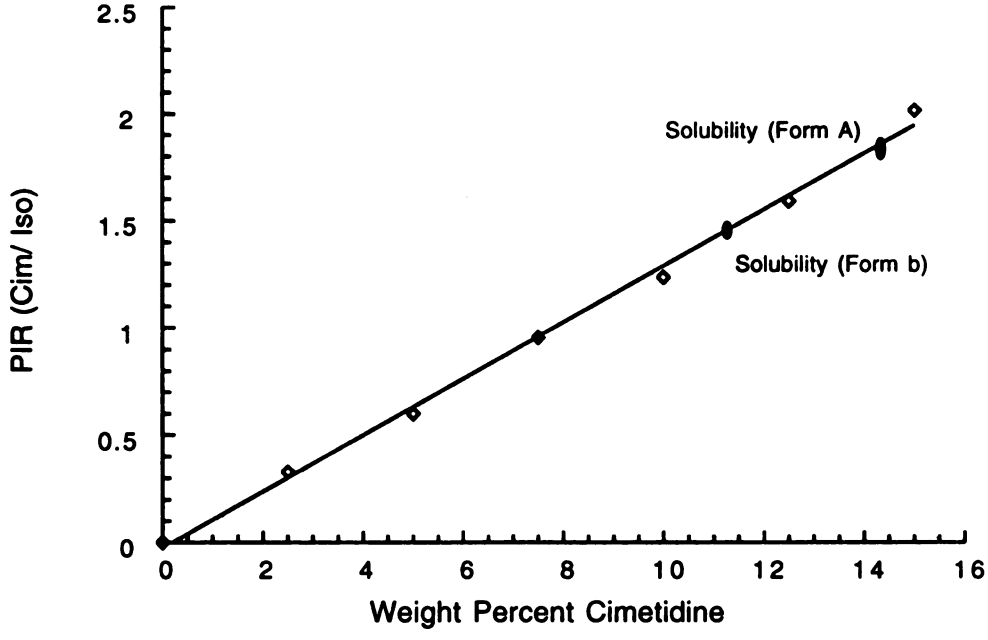

Figure 13: PIR's of 675 cm-1 (cim) to 494 cm-1 (isoprop) as a function of cimetidine concentration in 1.75/1 (v/v) isopropanol-water solutions. Solubilities are represented by ovals and calibration curve points are represented by squares. Excitation wavelength 647.12 nm, Temperature 25 °C.

Table 1: Conditions and results for phase transformation experiments done in isopropanol.

Temperature: 50 °C
Solvent: Isopropanol
Total Weight of Seeds: 0.30g
Total Volume of Solution Saturated w.r.t Form A: 45 ml

Weight % A	Weight % B	Complete Transformation to B?	Approximate Transformation Time	Approximate Time to Reach B Solubility
100	0	no	------	------
75	25	no	------	------
50	50	no	------	------
25	75	yes	10 hours	24 hours
0	100	-------	------	15 hours

Table 2: Conditions and results for phase transformation experiments done in 1.75/1 (v/v) isopropanol-water.

Temperature: 25 °C
Solvent: 1.75/1 (v/v) Isopropanol/Water
Total Weight of Seeds: 0.30g
Total Volume of Solution Saturated w.r.t Form A: 45 ml

Weight % A	Weight % B	Complete Transformation to B?	Approximate Transformation Time	Approximate Time to Reach B Solubility
100	0	no	------	------
99	1	yes	16 hours	24 hours
75	25	yes	1.5 hours	10 hours
50	50	yes	1.0 hour	10 hours
25	75	yes	30 minutes	10 hours
0	100	-------	------	10 hours

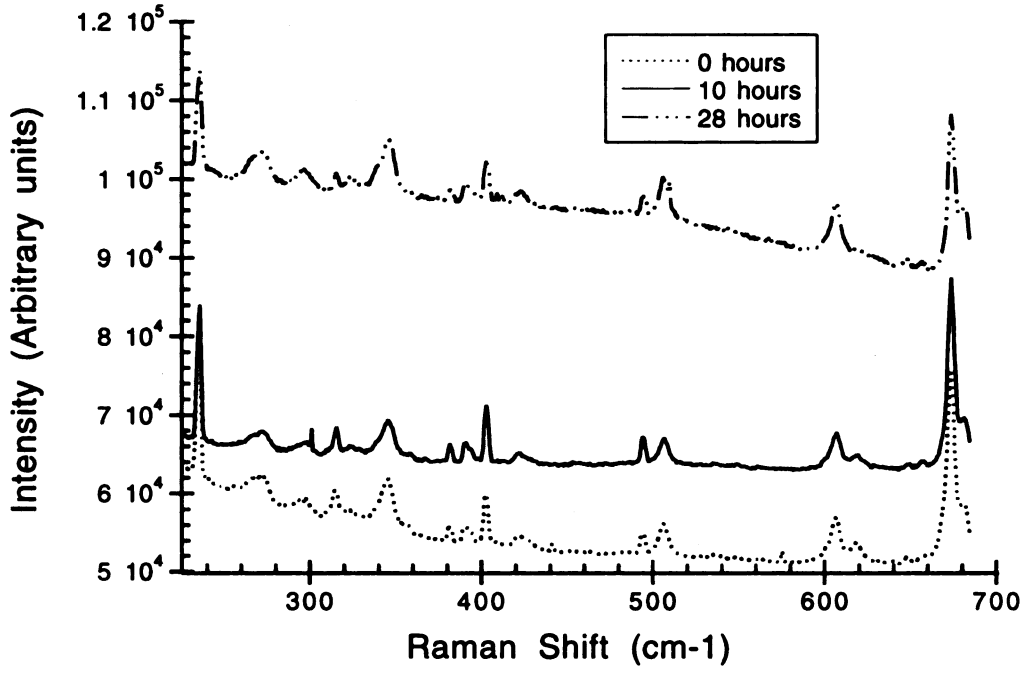

Figure 14: Solid state Raman spectral changes during phase transformation of cimetidine. Excitation wavelength 647.12 nm, Temperature 25 °C.

Two sets of experiments were run, one with isopropanol (Table I) as the solvent, and the other with 1.75/1.0 (v/v) isopropanol-water (Table II). Each set consisted of trials where the B/A ratio (w/w) varied from 0 to 100 percent, at 25% intervals. During the phase transformation, system changes were observed in the solid and solution phases. The solution PIR's for both experimental sets are shown as a function of time in Figures 10 and 11, while typical spectral changes in the solid state are shown in Figure 9. The solution PIR's were used to quantitatively measure cimetidine concentration while the solid state spectra were used to estimate the time of total phase transformation.

With isopropanol as the solvent, detectable phase transitions were only seen in the slurry starting with 75%B/25% A (Figure 10). This particular experiment resulting in a total transformation also had a change in solute concentration after the phase transformation was complete. For the conditions and results given in Table I, there must

be a large percentage of form B present to achieve total phase transformation. During phase transformation, the solute concentration remained at the saturation value of phase A until all of phase A had transformed to B. These results are consistent with those of Sudo et. al,[11] thus showing that the transformation is growth limited with respect to phase B.

The experiments with less than 75% B present in the initial slurry resulted in little or no detectable phase transformation, along with little or no changes in solute concentration. This is not to say that a phase transformation could not take place, but under the given conditions a phase transformation was not detectable in the 36 hour period of observation. Several reasons can be offered for this. The low solubility of cimetidine in isopropanol could have allowed the kinetically favored form A to exist for long periods of time in a slurry, despite the fact that the stable form B was present. The small difference in solubility of form A and form B gave a relatively small driving force for phase transformation. The dependence of total phase transformation upon the amount of form B present in the slurry also suggests that a secondary nucleation mechanism may play a larger role for a phase transformation in this system, since secondary nucleation has been shown to depend on solid phase content in a slurry.[17]

The constant or near constant solute concentration during phase transformation and the very slow approach to equilibrium in the trial runs with 75% B or more give support for a growth limited mechanism, which was discussed earlier and outlined in detail by Cardrew and Davey,[13] and also concluded by the Sudo et. al.[11]

When a mixed solvent of 1.75/1 (isopropanol/water) was used, the results were considerably different. Phase transformations occurred in all the experiments except the one run without phase B present in the initial slurry (Figure 11). The phase transformations were much faster than in isopropanol. A full transformation occurred in less than one hour for each experiment except for the slurry seeded with a 99% A/ 1% B

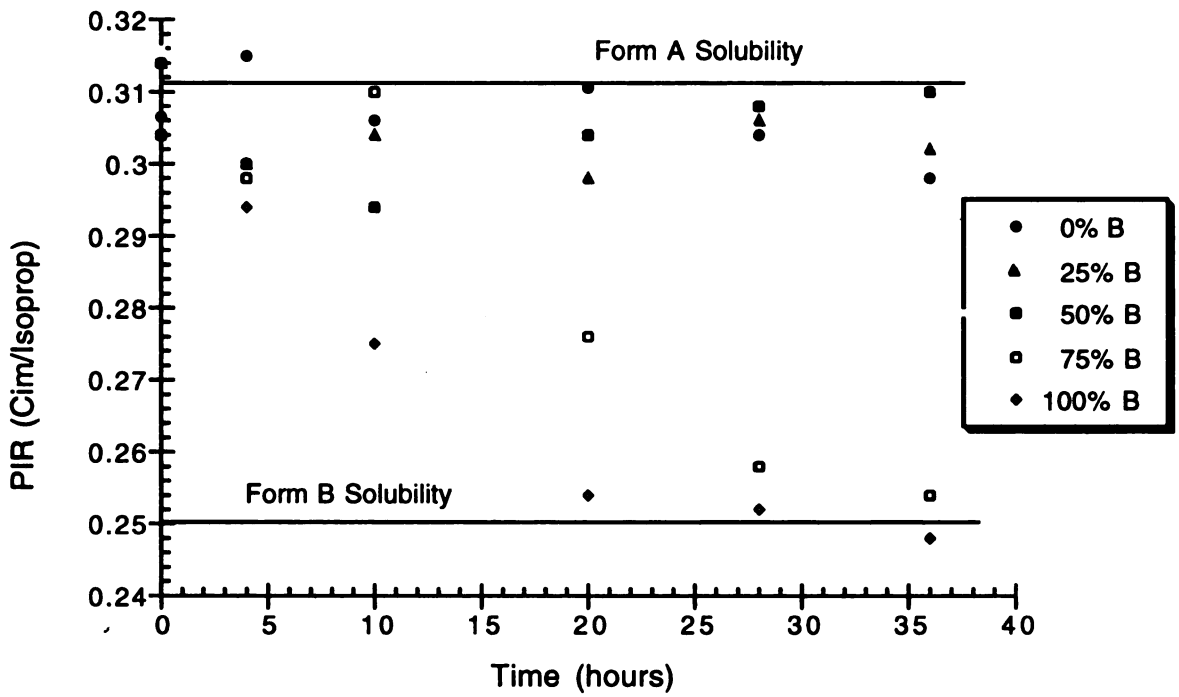

Figure 15: Change in PIR's of of 675 cm-1 (cim) to 494 cm-1 (isopropanol) during phase transformation experiments in isopropanol. Excitation wavelength 647.12 nm, temperature 50 °C.

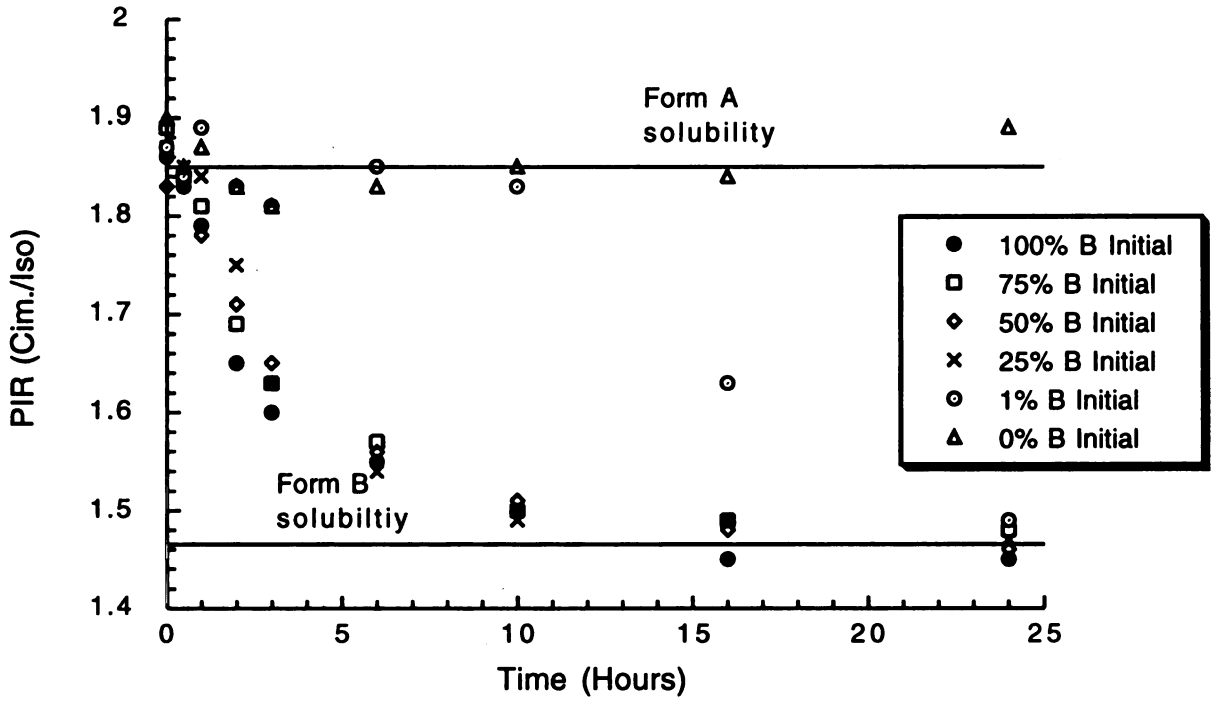

Figure 16: Change in PIR's of of 675 cm-1 (cim) to 494 cm-1 (isopropanol) during phase transformation experiments in 1.75 (v/v) isopropanol-water. Excitation wavelength 647.12 nm, temperature 25 °C.

mixture, where a full phase transformation occurred after 16 hours. The solute concentration curves as a function of time show that this transformation appears to be dissolution limited with respect to phase A.[13] The higher overall solubility and larger solubility differences between phases probably created a stronger driving force for phase transformation, thus creating conditions for a much quicker phase transformation than that seen with isopropanol as the solvent. Based on the shape of the solute concentration profiles, transformation kinetics appear to be dissolution limited, as opposed to the growth limited kinetics with isopropanol as the solvent.

2.4. *In Situ* Raman Spectra of Cimetidine Slurries

The largest advantage that Raman spectroscopy offers over more traditional analytical methods is that it can be used to observe system changes *in situ.* This eliminates the need to draw off sample aliquots, thus reducing the possibility of experimental error. When applied to a crystal slurry, *in situ* measurements offer the ability to determine conditions in the solid and the liquid phase simultaneously, while leaving the system intact.

In situ spectra of each phase in an agitated slurry of cimetidine saturated with respect to each polymorph are shown in Figure 12 and 13. Spectral characteristics of both the solid and liquid states can be seen in these graphs. The liquid state spectra of isopropanol show bands at 494 cm^{-1}, 425 cm^{-1}, and 375 cm^{-1}. The solid state spectra show several cimetidine bands in the 600 to 700 cm^{-1} region, the 300 to 350 cm^{-1} region, and the 100 to 200 cm^{-1} region. These experiments are preliminary and demonstrate the potential to use Raman spectroscopy as a tool for in situ analysis. Instrumentation improvements need to be implemented for Raman spectroscopy to be used for on-line analysis. Pallister et al. has coupled holographic notch filters to a single monochrometer,

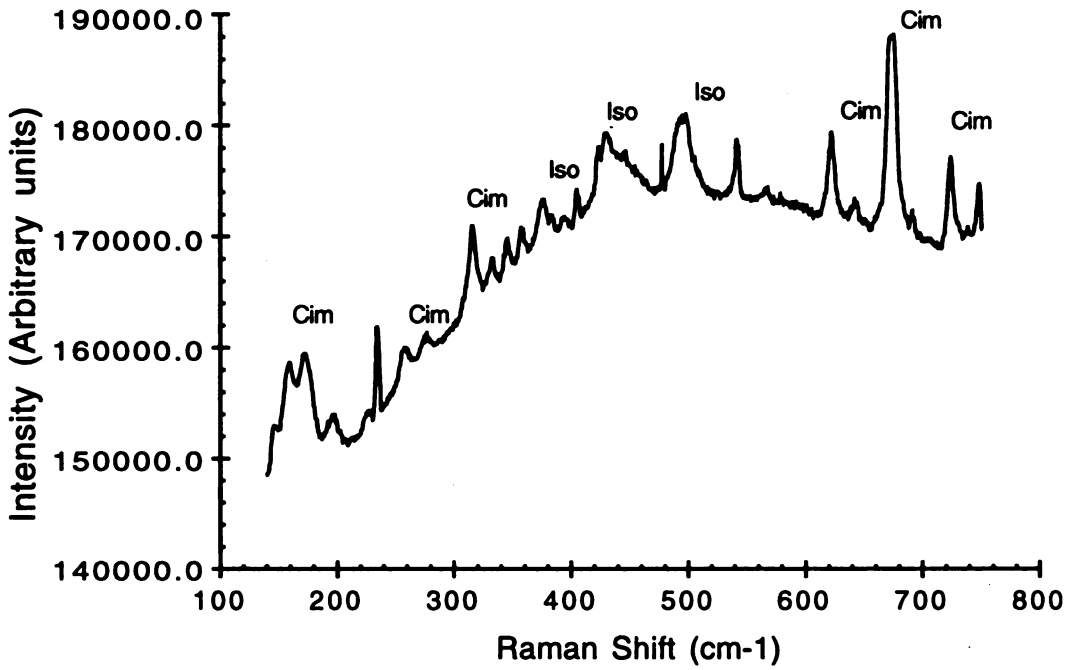

Figure 17: *In situ* Raman spectra of cimetidine form A in isopropanol. Excitation wavelength 647.12 nm, Temperature 25 °C.

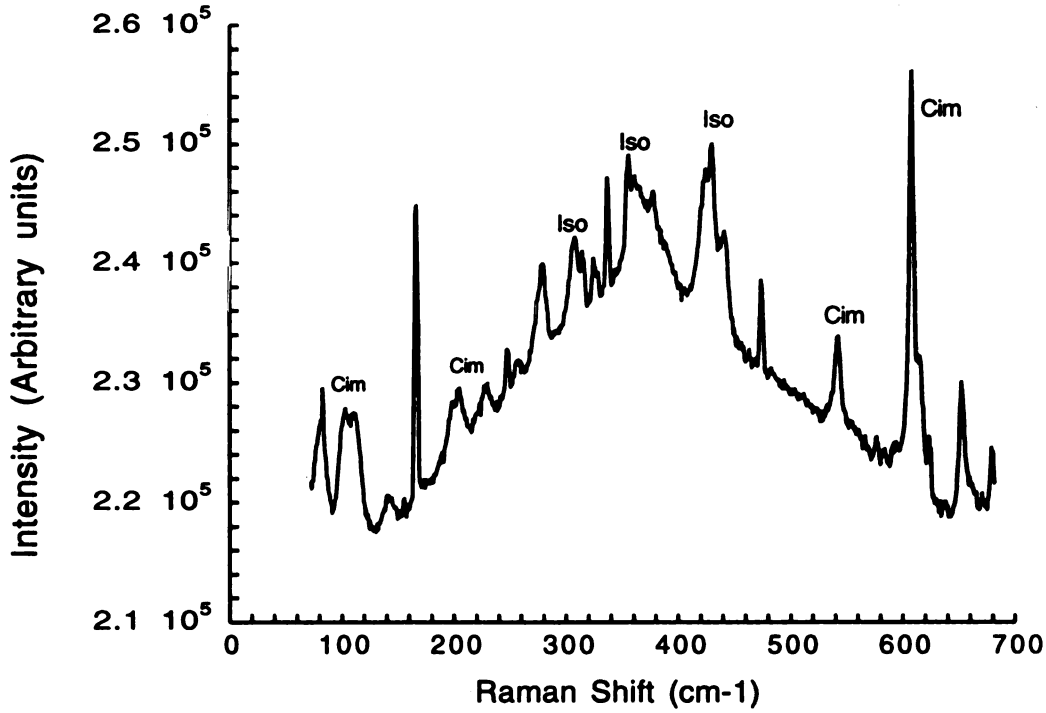

Figure 18: *In situ* Raman spectra of cimetidine form B in isopropanol. Excitation wavelength 647.12 nm, Temperature 25 °C.

increasing throughput by an order of magnitude over a Spex Triplemate while still maintaining Rayleigh light rejection.[18,19] This configuration gives better signal to noise ratios, thus reducing spectral accumulation times.

2.4. Summary and Conclusions

Raman spectroscopy can be used to investigate solvent-mediated phase transformations, and also shows promise as a tool to study crystalline slurries *in situ*. A Kr^+ ion laser using an excitation of 647.12 nm offers adequate signal to noise ratio while eliminating the problems of fluorescence associated with excitation of lower wavelength. The solid state spectra of cimetidine forms A and B show differences in the lattice vibration regions. These spectral differences suggest differences in crystal structure, but assignment of the lattice vibration bands for each polymorph must be done to confirm this. Spectra of cimetidine in solution show a linear dependence of the PIR between cimetidine (675 cm^{-1}) and isopropanol (494 cm^{-1}) on concentration of cimetidine. These spectral characteristics were used to observe the conditions during a solvent-mediated phase transformation for cimetidine in both the solid and solution phases.

Experiments with isopropanol as the solvent showed that the transformation from form A to form B is growth limited, and appears also to be dependent upon the density of form B in the crystal slurry, suggesting that secondary nucleation is important in isopropanol. Experiments with 1.75/1.0 (v/v) of isopropanol-water showed a solvent-mediated phase transformation from form A to form B that was dissolution limited, and occurred much faster than the transformations in isopropanol.

In situ Raman spectra of cimetidine slurries in isopropanol showed that spectral lines of forms A and B in the solid state can be distinguished from spectral lines of isopropanol in the liquid state. The instrumentation can be greatly improved by using

holograpic notch filters coupled to a single monochrometer. Once done, *in situ* Raman spectroscopy should be excellent for further phase transformation and crystallization studies, since it allows the observation of conditions without disruption of the system.

References

1. Solid State Chemistry of Drugs, S. R. Byrn (Academic Press, New York, 1982) pp. 29-58, 79-102.

2. J. K. Haleblian, *Journal of Pharmaceutical Sciences* **64** (1975) 1269.

3. M. A. Heathman, *Trends in Analytical Chemistry* **8** (1989) 19.

4. P. Van Houng, *Journal of Pharmaceutical and Biomedical Analysis* **4**(1986) 811.

5. Raman Spectroscopy in Biology, A. T. Tu (John Wiley and Sons, Inc., New York, 1982) p. 7.

6. Raman Spectra of Molecules and Crystals, M. M. Sushchinski, (Israel Program for Scientific Translations Ltd., New York, 1972) p. 83.

7. M. Shibata, et. all, *Journal of Pharmaceutical Sciences* **72** (1983) 1436.

8. S. Sudo, K. Soto, and Y. Harano, *Journal of Chemical Engineering of Japan* **24** (1991) 237.

9. B. Hegedüs and S. Görög, *Journal of Pharmaceutical and Biomedical Analysis* **3** (1985) 303.

10. B. Prodic-Kojic et. al., *Gazetta Chimica Italiana* **109** (1979) 535.

11. S. Sudo, K. Soto, and Y. Harano, *Journal of Chemical Engineering of Japan* **24** (1991) 628.

12. A. M. Tudor, et. al. *SpectroChimica Acta* **47A**(1991) 1389.

13. P. T. Cardrew and R. J. Davey, *Proceedings of the Royal Society of London* **A398**(1985) 415.

14. U. Bismayer, *Phase Transitions* **27** 211 (1990) 211.

15. Infrared and Raman Spectra of Crystals, G. Turrell, (Academic Press, London, 1972) pp. 159-167.

16. E. F. Gross and M. F. Vuks, *Nature* **135** (1935) 100, 431.

17. Theory of Particulate Processes, A. D. Randolph and M. A. Larson, (Academic Press, New York, 1971) pp 104-107.

18. D. M. Pallister, et. al., *Applied Spectroscopy*, **46**, (1992) 1469.

19. Kaiser Optical Product Literature, January 1995.

Chapter 3

The Use of Carminic Acid as a Trace Fluorescent Probe in Aqueous Sugar Solutions

3.1 Introduction

The molecular interactions that occur in supersaturated solutions is an essential part of understanding crystal nucleation and growth. Much work on understanding this phenomena has been done in this area in recent years. Previous investigators have studied the nature of molecular association and solute organization in supersaturated solutions using a variety of techniques. Myerson[1,2] undertook diffusion studies in a variety of electrolytes (NaCl, KCl) and non-electrolytes (urea, glycine, glycine-valine) indicating the formation of aggregates in solution. Garside and Larson[3,4] observed concentration gradients in isothermal columns of supersaturated citric acid, potassium sulfate, urea and sodium nitrate, which suggested solute structuring.

Attempts to characterize solute-solvent interactions in aqueous sugar solutions have been carried out using several methods. Allen[5] has done studies with sucrose similar to Garside and Larson which showed that isothermal columns of supersaturated solutions contained concentration gradients. Sugget[6] has used NMR and dielectric relaxation techniques to identify the interaction of water in sugar solutions, namely the presence of associated water and bulk water. Richardson, *et al.*[7] used ^{2}H and ^{17}O high field NMR to show water mobility in sucrose solutions as a function of concentration. Similarly, Hills[8] investigated the hydrogen exchange kinetics and water reorientation dynamics in aqueous glucose solutions.

The use of extrinsic fluorescent probes gives another method to determine solution structure. A recent investigation by Chakraborty and Berglund[9] using trace amounts of pyranine in aqueous sugar solutions showed that relative amounts of associated water and bulk water could be detected by monitoring the relative amount of protonated and

deprotonated forms in solution. By relating the emission intensities of the protonated and deprotonated forms, they showed that relative amounts of associated and bulk water can be determined in a given solution. The use of pyranine has been demonstrated to work well for the studies of water activity in aqueous sugar solutions but it is only a D and C approved dye, thus it is not allowed for direct application in foods.

In this study we investigated the use of carminic acid, a naturally occurring, F, D and C approved dye[10] as a substitute for pyranine in food applications. Its ground state electronic spectrum is known to be influenced by pH[11] and we found similar behavior in the excited state. As can be seen from Figure 19,[10] carminic acid has a glucose group in its structure, which may allow it to interact more easily with sugar molecules in an aqueous solution. The glucose structure may also allow it to function as a tailor-made impurity,[12] which will discussed in more detail below. These features suggest that carminic acid is a suitable indicator of solution properties.

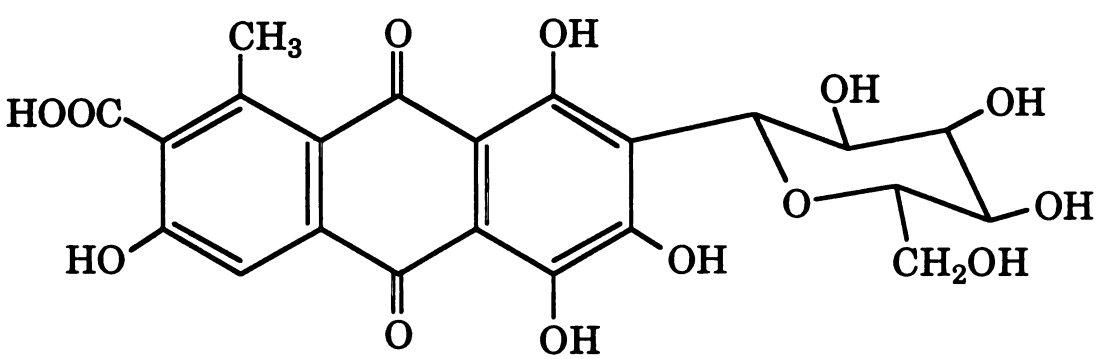

Figure 19: Chemical structure of carminic acid

Previously, carminic acid has been used to determine trace quantities of Boron in solution[13,14], and it has also been used in the spectrofluorimetric determination of several transition metal ions.[15,16,17] Carminic acid has also been used as a staining agent in histography.[18] It has also received considerable attention in the food industry as a red coloring agent.[19] When complexed with aluminum, it forms carmine, which can give color in the range from pale strawberry red to a dark blackcurrant red.[20] Carminic acid

undergoes ester hydrolysis in alkali solutions,[21] which accounts for its instability above pH 7.5. Allevi and coworkers completed[22] the first total synthesis of carminic acid.

3.2 Carminic acid as a tailor-made impurity

Carminic acid was also chosen because it is a glycoside, thus it may be able to function as a tailor-made impurity. A tailor-made impurity as defined in literature[12,23] is a special class of additives designed to interact with selected crystalline faces in very specific ways. These impurities have structural characteristics similar to the host molecule which allow it to be more easily incorporated into the lattice during crystallization. The fact that carminic acid has a glucose group makes it a candidate to function as a tailor-made impurity[12] in sucrose and glucose solutions. Generally, a tailor-made impurity is added to inhibit crystal growth and/or change the crystal morphology. This is due to dissimilarities between host and impurity that disrupt the normal crystallization process. In our study, we were able to use a very small amount of acid and still obtain intense spectra. With low probe concentration, (2.5 ppm) the change in crystal interface conditions would be kept to a minimum, but the high emission intensity would still allow monitorization of the crystallization process conditions at the crystal interface and the bulk solutions. Crystallization of aqueous sugar solutions are currently being carried out by Racemis and Blanchard.[21]

3.3 Materials and Methods

Absorption spectra were obtained using a Perkin Elmer Lambda 3A UV/Vis Spectrophotometer in conjunction with a Perkin Elmer R100A recorder. Emission Spectra were obtained with a Spex 1681 FLUOROLOG 2 0.22m Spectrometer. Four sided Suprasil quartz cuvettes with a 1 cm pathlength were used to contain the samples in both

absorption and emission. To aid in sugar dissolution, a Bransonic 220 sonic bath was used. All solution pH measurements were taken with an Orion Research digital analyzer / 501 and a combination electrode.

Ultra pure grade RNase-free sucrose (Baker Chemicals), reagent grade anhydrous glucose powder (Baker), carminic acid (Aldrich), and HPLC grade water (Fisher) were used. A stock solution of 4×10^{-4} M carminic acid was prepared with spectroscopic grade methanol (Malinckrodt). For emission fluorescence studies, solutions of 2.5 ppm carminic acid were prepared. For absorption studies, solutions of 5 ppm were made. Before each solution was prepared, the amount of carminic acid necessary for a given concentration was calculated. The proper amount of stock solution was then calculated and placed into a 20 ml vial with a precision pipette. The stock was allowed to evaporate, thus giving the proper amount of probe. Each vial containing dry carminic acid was set aside and kept away from light.

The sugar solutions were prepared to weigh exactly 10 grams. (±0.01%) The sucrose samples varied in weight percent from 20% to 75%, with a saturation point of 67% at 25 C, whereas the glucose solutions varied from 30% to 75%, with a saturation point of 48% at 25 C. The samples were prepared in 10% increments up to 60%. Above 60%, they were incremented by 5% in order follow changes in the supersaturated regions more closely. In preparation it was absolutely necessary to ensure complete dissolution of both sucrose and glucose solutions by heating and agitation.

After each solution was dissolved, it was quickly transferred into a vial with pre-evaporated carminic acid stock solution, and allowed to cool to room temperature. To insure homogeneous mixing of carminic acid, each cooled solution was reheated in the water bath for one minute, and allowed to cool again to room temperature. Solutions that were not reheated had visible and unwanted concentration gradients. Once the solutions reached room temperature, spectrophotometric readings were taken.

Fluorescence emission of carminic acid in aqueous glucose and sucrose solutions was measured using excitation wavelengths of 500 nm and 310 nm. The emission was monitored from 530 nm to 700 nm for samples excited at 500 nm, while the emission was monitored from 400 nm to 700 nm for samples excited at 310 nm. Excitation and emission slit widths of 2 mm were used for all spectra. For each sample, a background spectrum was taken of the corresponding sugar-water solution. Samples were background corrected by subtracting the fluorescence emission spectrum of each aqueous sugar solution .

Absorption spectra of carminic acid-doped sugar solutions was followed from 250 nm to 600 nm. For both sugars, a scanning speed of 120 nm/min. was used. The pH of each solution was measured.

.

3.4 Results and Discussion

The absorption spectra of carminic acid in aqueous sugar solutions was determined first to ascertain excitation wavelengths and also to determine the species that existed in the ground state. The spectra of carminic acid in aqueous glucose solutions are shown in Figure 20. Based on the work done by Schwing-Weil,[11] the visible absorption spectra indicate that carminic acid can exist in the LH_3, LH_2^-, and LH^{-2} states. In samples containing less than 60% glucose, carminic acid exists as a mixture of LH^{-2} and LH_2^- states, whereas in solutions with concentrations higher than 60% glucose, carminic acid exists in the LH_3 species. Comparing these spectra to that of buffer solutions with similar pH, it appears that visible absorption spectral changes in the ground state are a function of glucose solution pH. The UV region of the absorption spectrum shows an equilibrium between a species absorbing at 325 nm and a species absorbing at 280 nm that is a function of glucose concentration. The assignment of these bands is as yet undetermined, but it is being investigated.[21]

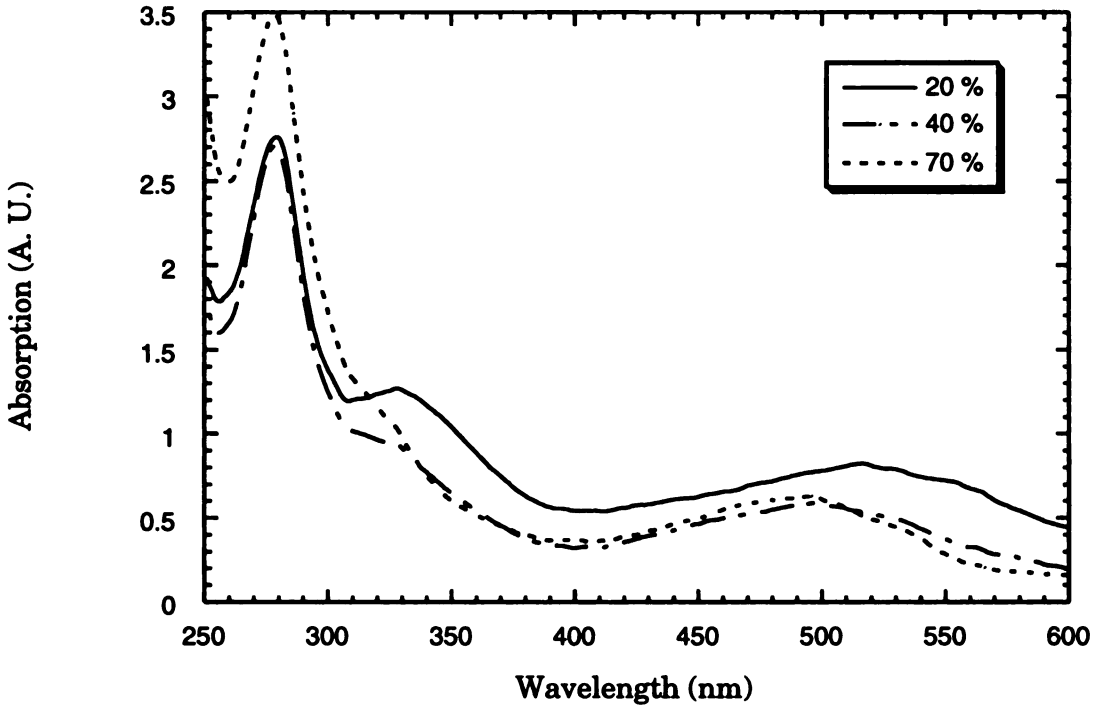

Figure 20: Absorption spectra of carminic acid in aqueous glucose solutions. Carminic acid concentration 5 ppm, temperature 25 °C.

The spectra of carminic acid in aqueous sucrose solutions is shown in Figure 21. There is little or no variance in the visible absorption spectra as a function of sucrose concentration. In aqueous sucrose solutions, carminic acid exists in the L^{-3} and LH^{-2} states. When these spectra are compared to those of buffer solutions with comparable pH's, they appear to have spectra that is not dependent on pH. The fact that the sucrose solution pH changes by two units as a function of sucrose concentration with no corresponding change in visible absorption spectra further exemplifies this. In a larger sense, it implies that the carminic acid molecule in the ground state exists in one kind of environment that is independent of sucrose concentration. Similar to carminic acid in aqueous glucose solutions the UV absorption in aqueous sucrose solutions spectra show an equilibrium between the species absorbing at 325 nm and the species at 280 nm that is a function of sucrose concentration.

The emission spectra of carminic acid in both sugars was done using excitation wavelengths of 500 nm and 310 nm. These excitation wavelengths were chosen based on

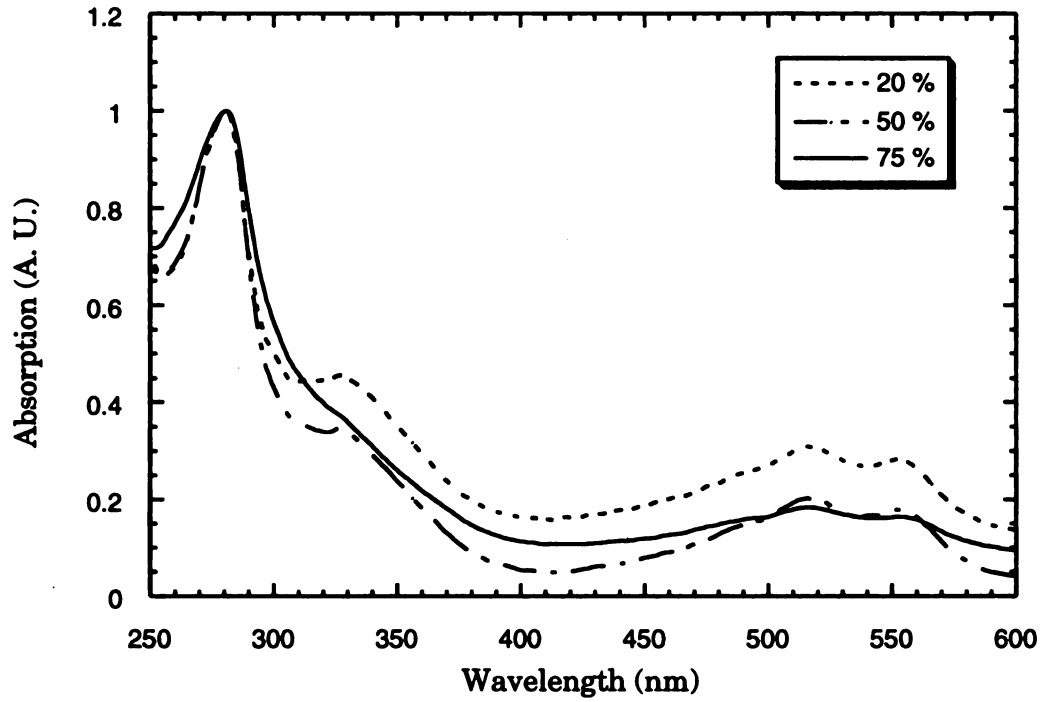

Figure 21: Absorption Spectra of carminic acid in aqueous sucrose solutions. Carminic acid concentration 5 ppm, temperature 25 °C.

the UV-visible spectra of the sugars which showed isosbestic points at 310 nm and 500 nm in the ground state.

Tentative band assignments of carminic acid in the excited state were made based on the visible emission spectra in buffer solutions. In 1M HCl, the fully protonated state (LH_3*) emits at 594 nm. In 1M NaOH, the fully deprotonated state (L^{-3}*) emits at 645 nm. It also appears that the LH_2^{-}* species emits at 610 nm and 450 nm, and the LH^{-2}* species emits at 580 nm. A full photochemical characterization of carminic acid is presently being undertaken, but for the purposes of this study we used the fore-mentioned band assignments. Similar to pyranine in sugar solutions[9], carminic acid indicates an equilibria between different microenvironments which can be used to determine sugar concentration, especially in the supersaturated region.

Emission spectra of carminic acid in solutions of varying glucose concentration using an excitation of 500 nm are shown in Figure 22. The results show an exponential

increase in the peak intensity ratio (PIR) between 594 nm and 610 nm as glucose concentration is increased and carminic acid concentration is held constant.

In Figure 23, the emission spectra of carminic acid in solutions of varying glucose concentration using an excitation of 310 nm are shown. The PIR between 594 nm and 450 nm show a much stronger exponential dependence than that seen between 594 nm and 610 nm. There also appears to be a clear isosbestic point at 525 nm, indicating an equilibria between two species of carminic acid as a function of glucose content.

According to Hill,[8] there are two types of water that can exist in an aqueous glucose solution. These are bulk water and solvation water. Bulk water refers to water that is not hydrogen bonded to a glucose molecule. Solvation water refers to water that is bound to a glucose molecule. The bulk water is capable of proton exchange. whereas the solvation water is not. Using a context similar to Chakraborty and Berglund,[9] we can refer to a micro environment where there is either a presence or absence of exchangeable protons in the vicinity of carminic acid. The presence of exchangeable protons would cause carminic acid to exist as the $LH^{-2}*$ species, thus emitting at 610 or 450 nm, whereas the absence of exchangeable protons would cause carminic acid to exist as the LH_3*, thus emitting at 594 nm.

In undersaturated aqueous glucose solutions at room temperature, Hill[8] calculated that there are 10 water molecules which surround a solvated glucose molecule. This model assumes that each glucose hydroxyl group is hydrogen bonded by two water molecules in solution. Since the solvation water is incapable of proton exchange, carminic acid residing near the glucose molecule would exist in the LH_3* state and thus emit at 594 nm. Carminic acid residing in the bulk water would be in an area suitable for proton exchange, thus it would emit in the $LH^{-2}*$ state of 610 nm or 450 nm.

In Figure 24, the PIR of 594 nm to 610 nm is shown. From this, it can be seen that the PIR is a function of glucose concentration, and thus a function of solvation and bulk water content, where emission at 610 nm would represent solvation water and

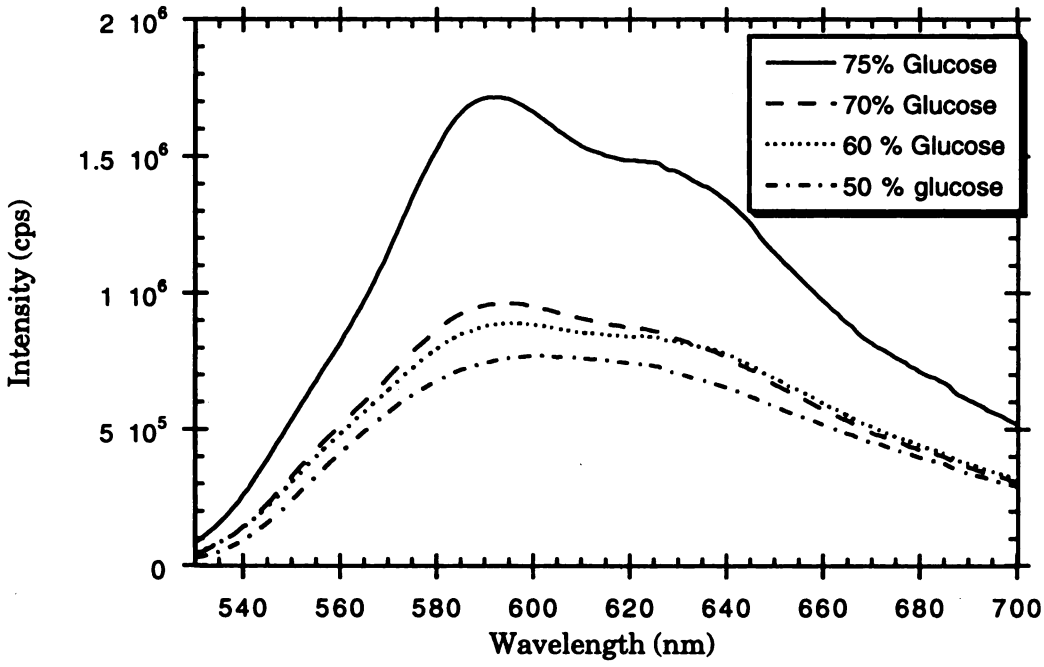

Figure 22: Emission spectra of carminic acid in aqueous glucose solutions. Carminic acid concentration 2.5 ppm, excitation wavelength 500 nm, temperature 25 °C.

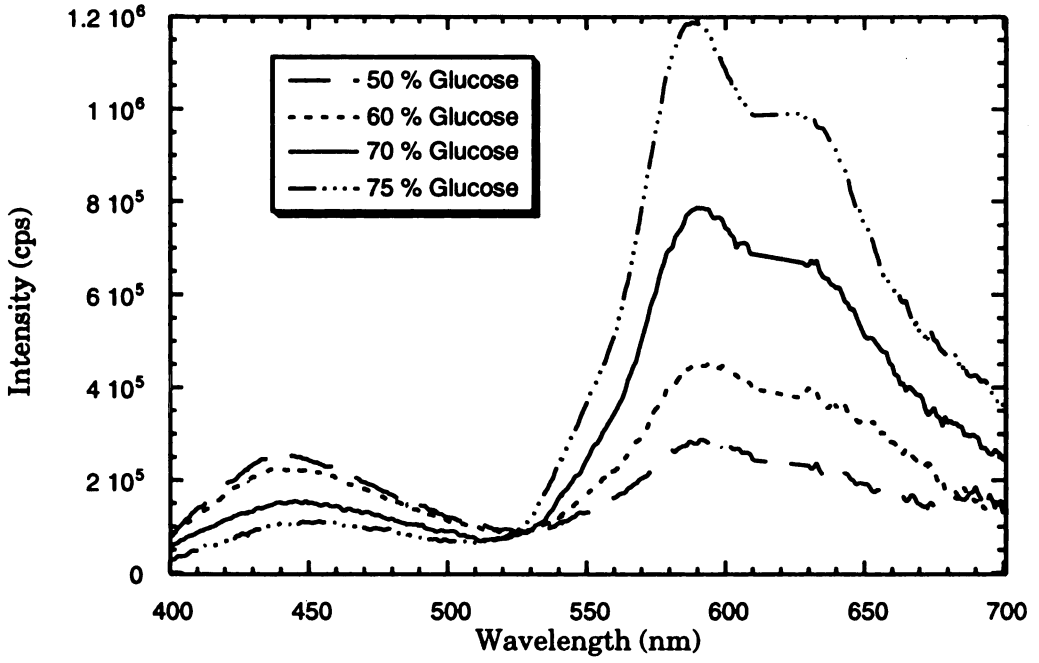

Figure 23: Emission spectra of carminic acid in aqueous glucose solutions. Carminic acid concentration 2.5 ppm, excitation wavelength 310 nm, temperature 25 °C.

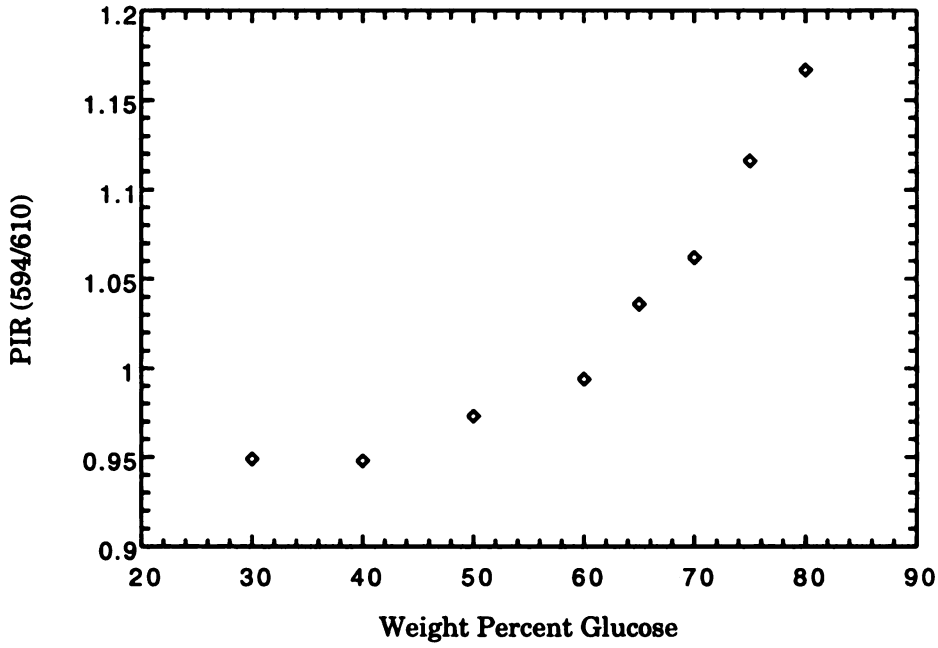

Figure 24: PIR's (594 nm/ 610 nm) of carminic acid emission in aqueous glucose solutions. Carminic acid concentration 2.5 ppm, excitation wavelength 500 nm, temperature 25 °C.

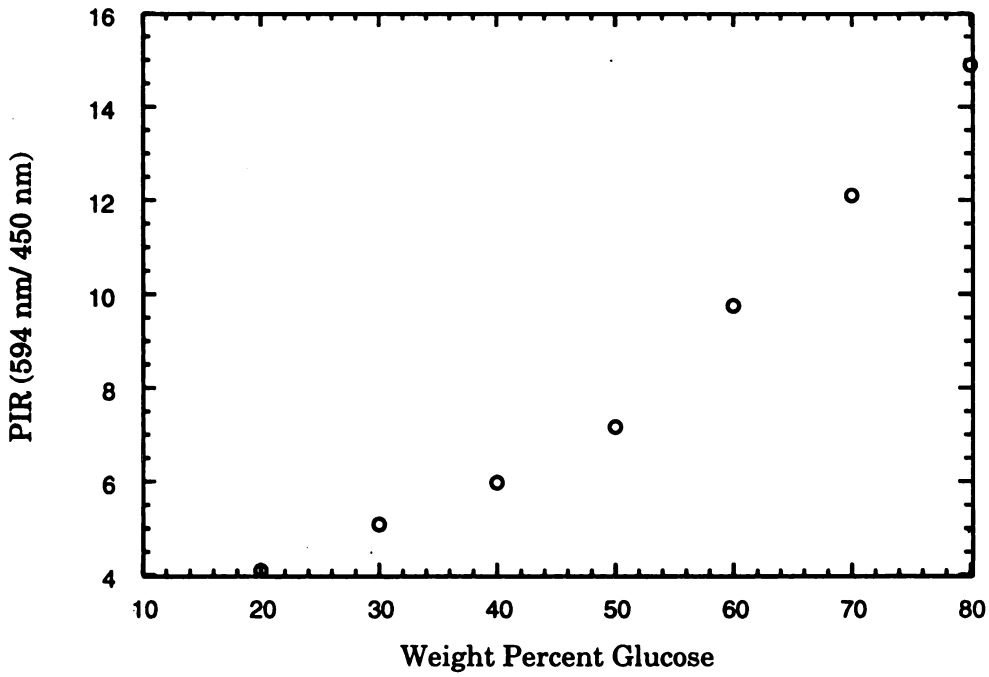

Figure 25: PIR's (594 nm/ 610 nm) of carminic acid emission in aqueous glucose solutions. Carminic acid concentration 2.5 ppm, excitation wavelength 310 nm, temperature 25 °C.

emission at 594 nm would represent bulk water. At around 50% concentration, there is a change in slope of the PIR. This occurs at about the saturation point of glucose in water at 25 °C. At this point, there is no longer enough water in solution for each respective glucose molecule to be hydrogen bonded by 10 water molecules.

Figure 25 shows the PIR of 594 nm to 450 nm. This show a much stronger dependence of PIR on glucose concentration. Similar to the above analysis, the emission seen at 594 nm represents solvation water and emission seen at 450 nm represents bulk water. There is also a change in slope of the PIR near the saturation point of glucose in water.

Since carminic acid is a known pH indicator[10,11], the pH's of each glucose solution was taken. The pH readings were the same for samples with and with out carminic acid. The results given in Figure 6 show that the pH decreases linearly from 6.4 (30% glucose) to 4.4. (75% glucose) Thus, it could be possible to assume that the change in emission spectra with respect to glucose concentration could be a function of pH and not glucose concentration. By comparing the emission spectra of the glucose solutions to emission spectra of buffer solutions with similar pH's, spectral differences are seen between glucose solutions and buffer solutions. Figure 27 shows the PIR's (594 nm to 610 nm) of carminic acid-doped glucose solutions along with the intensity ratios of buffer solutions with similar pH's. From this, the PIR's are similar to the buffer solutions in the under saturated regions, (up to 50% glucose) but once the solutions become supersaturated, their PIR show a positive, exponential deviation from that of the buffer solutions with the same pH. This deviation is probably due to the glucose content of the aqueous solutions, which would decrease carminic acid's ability to exchange protons and exist in a deprotonated state. The possibility of a pH effect was also investigated for solutions that were excited at 310 nm. Figure 28 shows the PIR's (594 nm to 450 nm) of carminic acid-doped glucose solutions along with the PIR's of buffered carminic acid solutions of similar pH. From

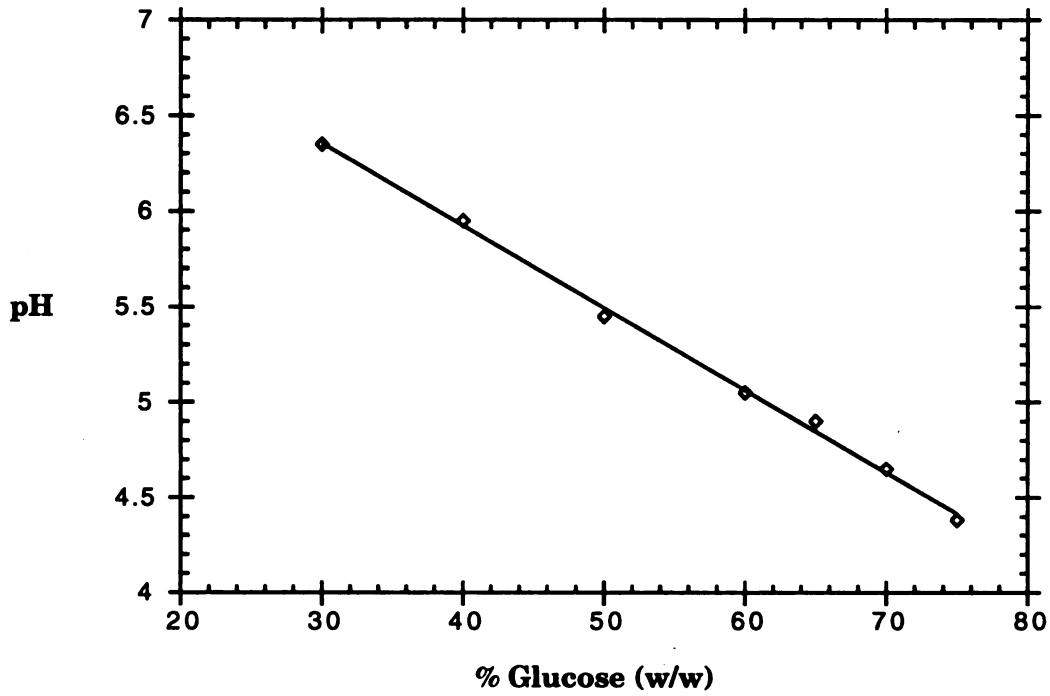

Figure 26: pH of glucose solutions as a function of glucose concentration. Carminic acid concentration 2.5 ppm, temperature 25 °C.

this it is clear that in the supersaturated region there is no effect of pH, and that the spectral changes seen are due to glucose content.

Previous work with sucrose has shown that there are two types of exchangeable protons in aqueous sucrose solutions.[6] This again would imply that there are two types of micro environments in which the carminic acid can exist, one as a protonated species and the other as a deprotonated species. Richardson *et al.*[7] showed through NMR water mobility studies in aqueous sucrose solutions that samples up to 40 weight percent sucrose contained water that was primarily free water, which is capable of proton exchange. At about 40 weight percent, the water mobility drops sharply, thus causing the proton exchange ability to decrease. In the first region, water would have the ability to exchange protons, thus carminic acid would exist in the deprotonated state. In the second region, there would be less likelihood for water to be able to exchange protons, thus, carminic acid would be more likely to exist in the protonated state. Based upon this and the emission

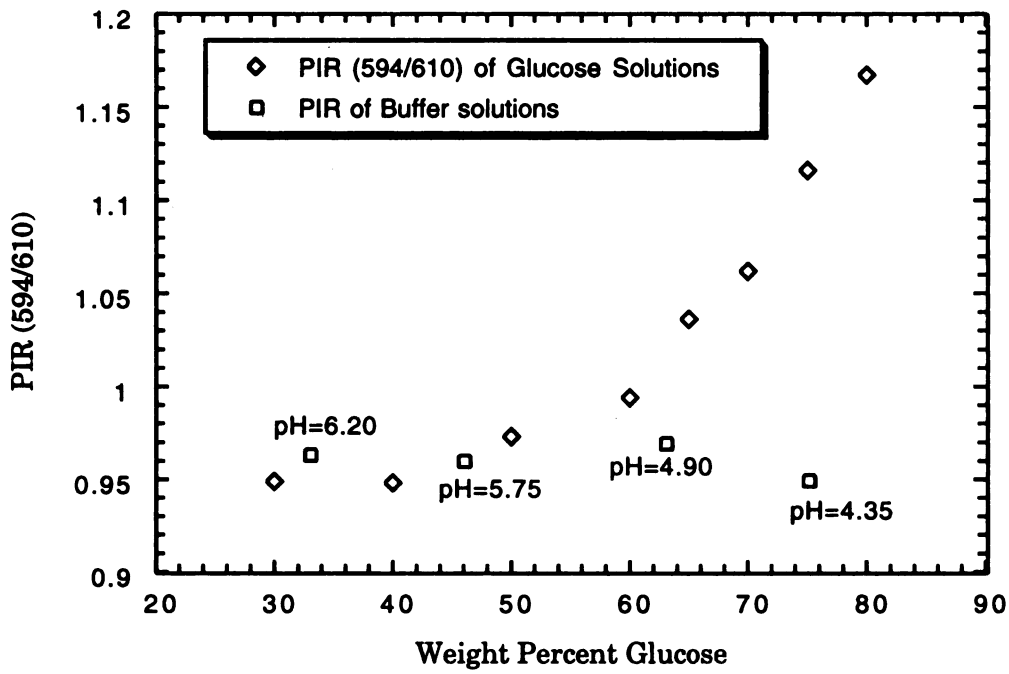

Figure 27: Comparison of carminic acid PIR's in aqueous glucose solutions and buffer solutions. Carminic acid concentration 2.5 ppm, excitation 500 nm, temperature 25 °C.

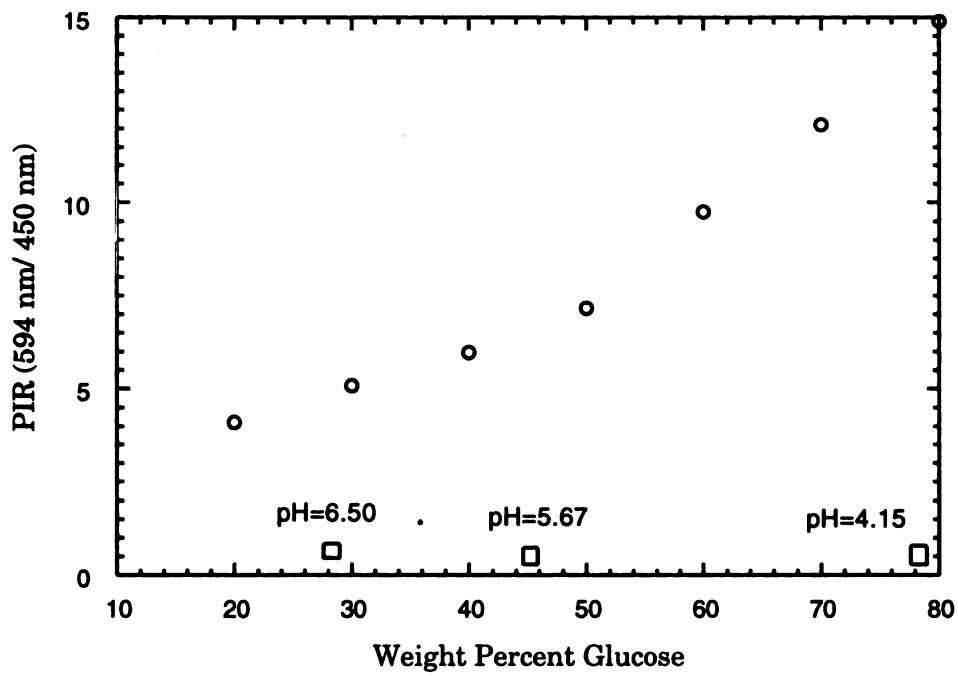

Figure 28: Comparison of carminic acid PIR's in aqueous glucose solutions and buffer solutions. Carminic acid concentration 2.5 ppm, excitation 310 nm, temperature 25 °C.

spectra of carminic acid in aqueous glucose solutions results discussed earlier, it appeared that carminic acid-doped sucrose solutions would give similar results to that of glucose.

The emission spectra of carminic acid-doped aqueous sucrose solutions are different than those seen with carminic acid in aqueous glucose solutions. When excited at 500 nm, carminic acid emits in the LH_2^{-*} state or the LH^{-2*} state, whereas solution excited at 310 nm emit from the LH_3^* state or the LH^{-2*} state. The sucrose emission spectra are given in Figure 29 and 30. Figure 29 shows spectra of carminic acid in aqueous sucrose solutions excited at 500 nm whereas Figure 30 shows spectra of carminic acid in aqueous sucrose solutions excited at 310 nm. The solutions excited at 500 nm show species that emit at 580 nm and 610 nm while the solutions excited at 310 nm show species that emit at 600 nm and 450 nm. Samples excited at 500 nm gave an increase in intensity with respect to increasing sucrose concentration whereas samples excited at 310 nm showed large changes in spectral characteristics as a function of sucrose content.

Figure 31 shows that there is very little change in fluorescence PIR between 580 nm and 610 nm (excitation 500 nm). Based on this, the amount of LH_2^{-*} and LH^{-2*} species in solution remains the same throughout the concentration range studied when an excitation wavelength of 500 nm is used. Figure 32 gives the PIR between 594 nm and 450 nm when an excitation of 310 nm is used. Assuming that the emission at 594 nm represents the LH_3^* form of carminic acid and the emission at 450 nm represents LH_2^{-*} form of carminic acid, then Figure 32 illustrates how the lack of bulk water forces carminic acid to exist in the fully protonated form as the sucrose concentration is increased. As with glucose, the possibility of a pH effect on the emission spectra of sucrose solutions was investigated. The pH's of each respective sucrose solution were taken, and are shown in Figure 33. They range from 8.6 (20% sucrose) to 6.5. (75% sucrose) Figure 34 compares the PIR's of sucrose solutions to that of buffer solutions with similar pH's when an excitation of 500 nm was used. From this it can be seen that the sucrose solutions have

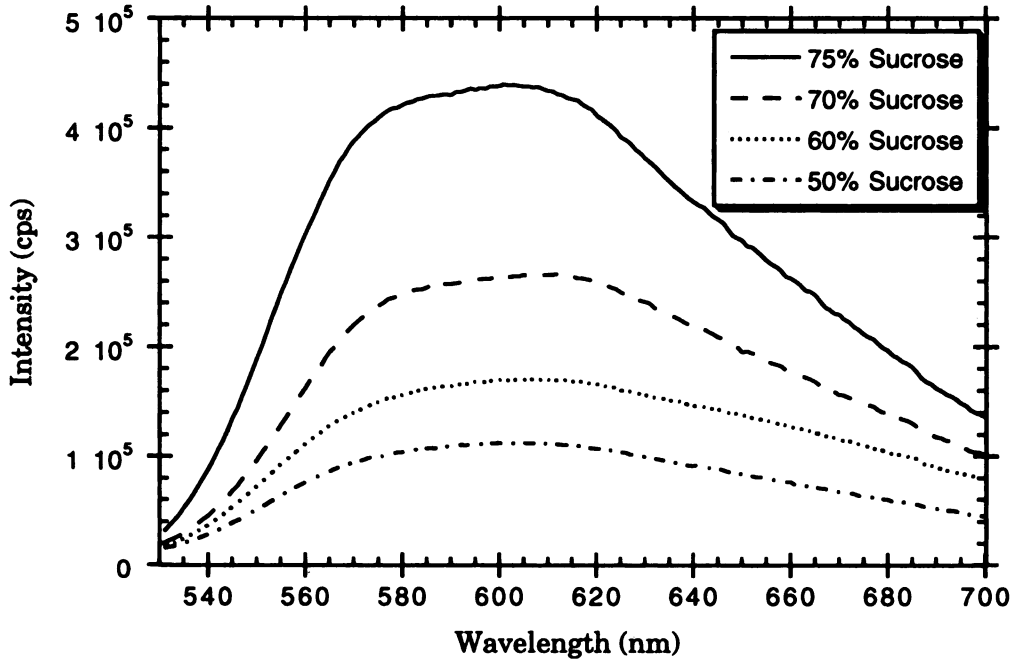

Figure 29: Emission spectra of carminic acid in aqueous sucrose solutions. Carminic acid concentration 2.5 ppm, excitation wavelength 500 nm, temperature 25 °C.

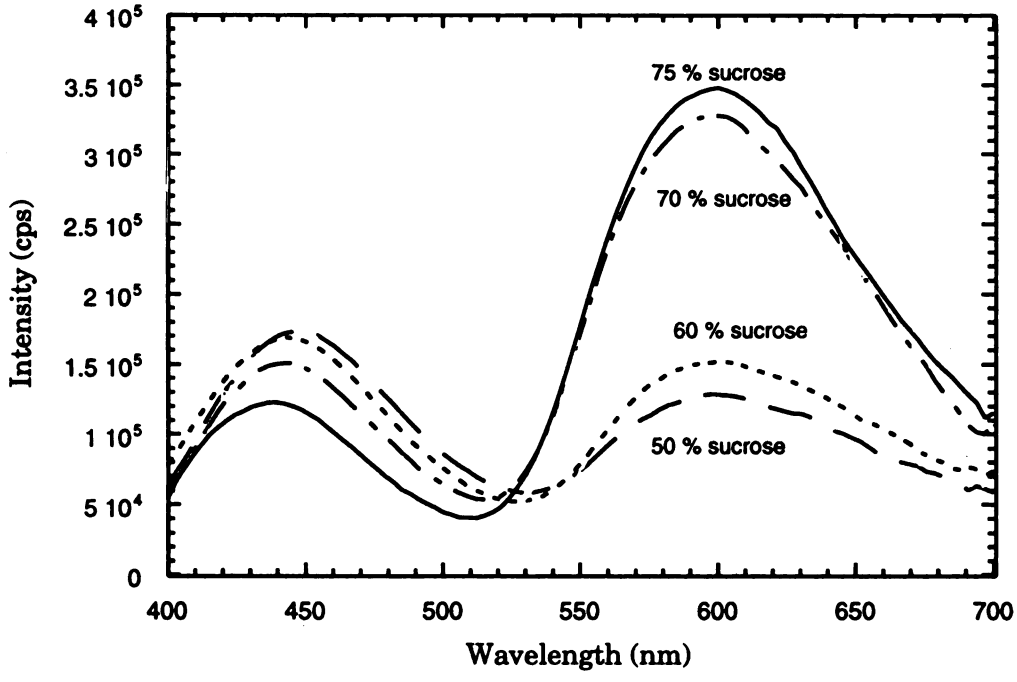

Figure 30: Emission spectra of carminic acid in aqueous sucrose solutions. Carminic acid concentration 2.5 ppm, excitation wavelength 310 nm, temperature 25 °C.

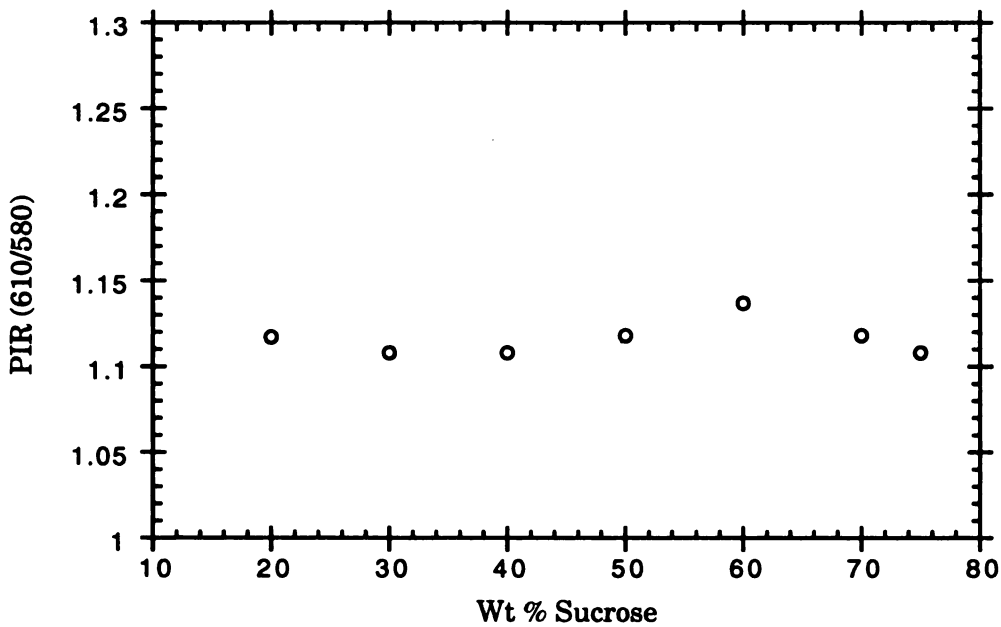

Figure 31: PIR's (610 nm/ 580 nm) of carminic acid emission in aqueous sucrose solutions. Carminic acid concentration 2.5 ppm, excitation wavelength 500 nm, temperature 25 °C.

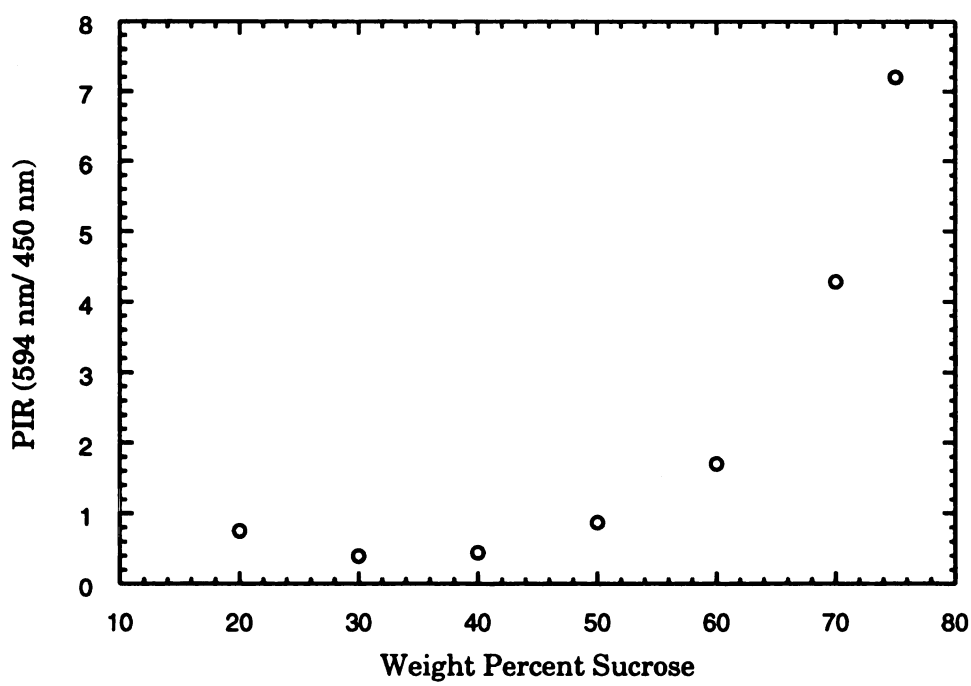

Figure 32: PIR's (594 nm/ 450 nm) of carminic acid emission in aqueous sucrose solutions. Carminic acid concentration 2.5 ppm, excitation wavelength 310 nm, temperature 25 °C.

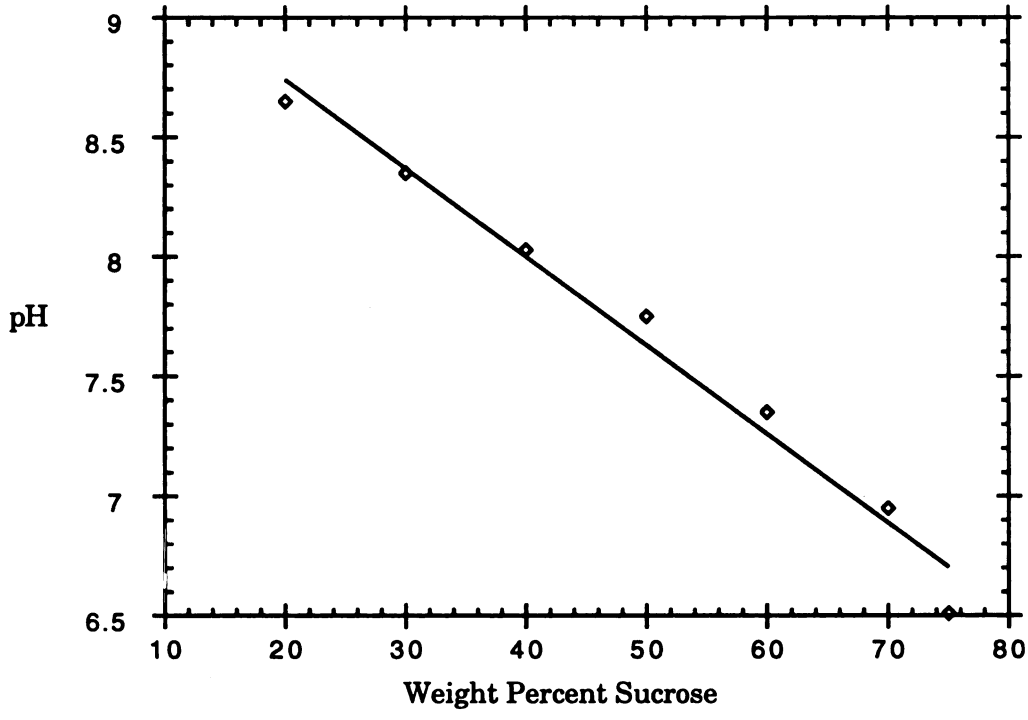

Figure 33: pH of glucose solutions as a function of glucose concentration. Carminic acid concentration 2.5 ppm, temperature 25 °C.

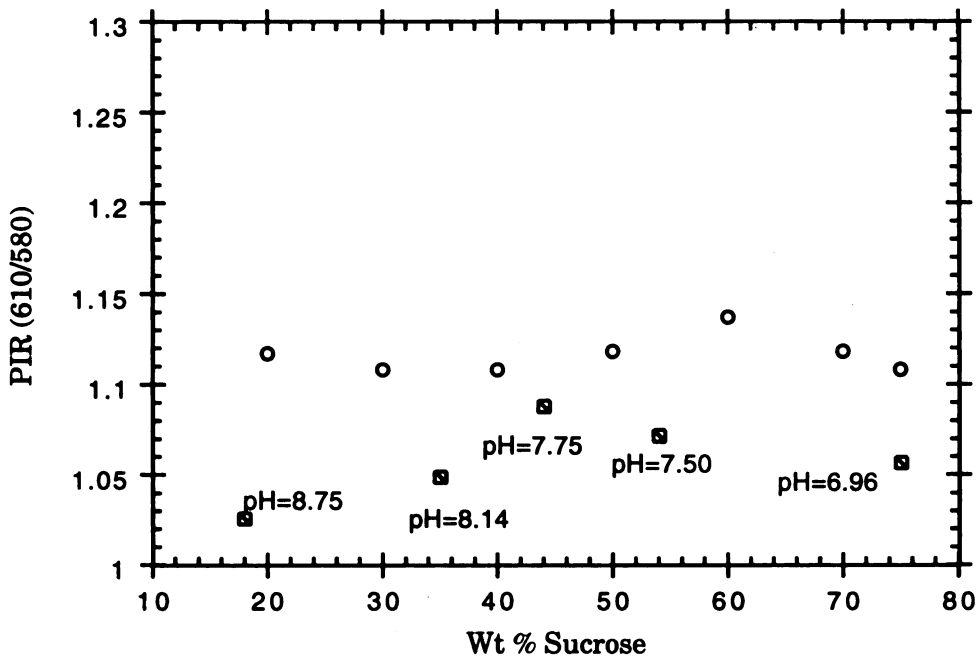

Figure 34: Comparison of carminic acid PIR's in aqueous sucrose solutions and buffer solutions. Carminic acid concentration 2.5 ppm, excitation wavelength 500 nm, temperature 25 °C.

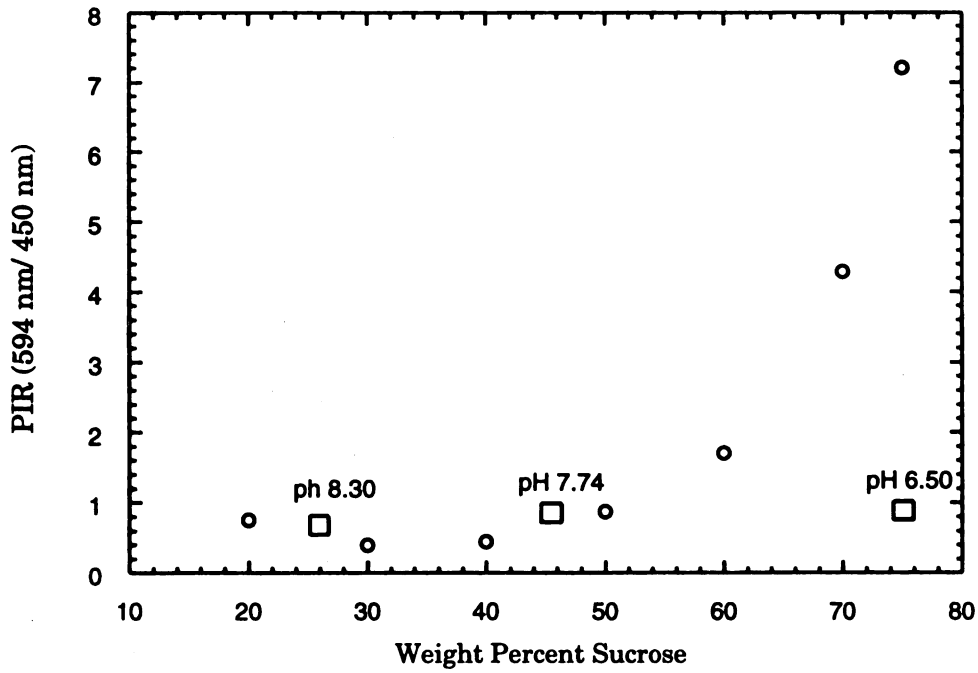

Figure 35: Comparison of carminic acid PIR's in aqueous sucrose solutions and buffer solutions. Carminic acid concentration 2.5 ppm, excitation wavelength 310 nm, temperature 25 °C

different PIR's than that of buffer solutions with similar pH's, thus showing that spectra seen with sucrose solutions is a result of sucrose content and not solution pH. The same analysis done on solutions excited at 310 nm (Figure 35) shows that there is no dependence of PIR on pH, thus it appears that in both cases, the spectral changes are dependent on sucrose concentration

3.5 Summary and Conclusions

Trace amounts of carminic acid (2.5 ppm) can be used as a fluorescent probe to measure solute concentration in aqueous glucose and sucrose solutions in a manner similar to that done with pyranine. The possibility of a pH effect was considered, with spectral differences being attributed to solution sugar content. An excitation of 500 nm and 310 nm was used for each set of solutions.

In aqueous glucose solutions, an excitation of either 500 nm or 310 nm can be used. For an excitation of 310 nm, the PIR of carminic acid between 594 nm (LH_3*) and 610 nm (LH_2^-*) shows an exponential dependence upon glucose concentration. Along with this, the fluorescence intensity increases as a function of glucose concentration. For an excitation of 310 nm, the PIR between 594 nm (LH_3*) and 450 nm (LH_2^-*) shows a very strong exponential dependence upon glucose concentration. In aqueous sucrose solutions an excitation of 500 nm shows little or no change in PIR between 610 nm (LH_2^-*) and 580 nm (LH^{-2}*) as a function of sucrose concentration, whereas an excitation of 310 nm shows a strong dependence of the PIR between 594 nm (LH_3*) to 450 nm (LH_2^-*) on sucrose concentration.

The visible absorption spectra of carminic acid in aqueous glucose solution indicates that carminic acid exists in the LH_2- and LH^{-2} states in undersaturated solutions and in the LH_3 state in supersaturated solutions. The visible absorption spectra of carminic acid in aqueous sucrose solutions indicates that carminic acid exists in the LH^{-2} and L^{-3}

with no change as a function of concentration. Ultraviolet absorption spectra showed and equilibrium between species at 325 nm and 280 nm for aqueous solutions of both sugars, but these species are yet to be identified.

Carminic acid appears to be a good candidate to determine glucose and sucrose concentration as a trace fluorescent probe. It has a high fluorescence intensity at low concentrations (2.5 ppm) making it easy to use, and a benign effect upon ingestion, making it acceptable for use in food and drugs. More work, both theoretical and experimental needs to be done to verify exactly how and why carminic acid acts in sugar solutions.

References

1. A. S. Myerson and L.S. Sorrel, *AIChe Journal* , **28**, (1982) 778.

2. A. S. Myerson and Y.C. Chang in: Industrial Crystallization, '84, Ed. S. J. Jancic and E. J. Jong (Elsevier, Amsterdam, 1984) p. 27.

3. M. A. Larson and J. Garside, *Chemical Engineering Science* , **41**, (1986) 1285.

4. M. A. Larson and J. Garside, *Journal of Crystal Growth*, **76**, (1986) 88.

5. A. T. Allen et. Al, *Nature*, **235**, (1972) 236.

6. A. Suggett and A. H. Clark, *Journal of Solution Chemistry*, **5**, (1976) 1.

7. S. J. Richardson, I. C. Baianu, and M. P. Steinberg, *Journal of Food Science*, **52**, (1987) 806.

8. B. P. Hills, *Molecular Physics*, **72**, (1991) 1099.

9. R. Chakraborty and K. A. Berglund, *Journal of Crystal Growth*, **130**, (1993) 587.

10. The Merck Index, Eds. S. Budavari, M. J. O'Neil, A. Smith and P. E. Heckelman (Merck & Co. Inc., 1989) p 280.

11. M. J. Schwing-Weill, *Analusis*, **14**, (1986) 290.

12. S. N. Black, R. J. Davey, and M. Halcrow, *Journal of Crystal Growth*, **79**, (1986) 765.

13. R. C. Calkins and V. A. Stenger, *Analytical Chemistry*, **28**, (1956) 399.

14. J. Anarez, A. Ferrer, J. M. Rabadan and L. Marco, *Talanta*, **32**, (1985) 1156.

15. G. F. Kirkbright, T. S. West, and C. Woodward, *Talanta*, **13**, (1966) 1637.

16. Poluektov, R. S. Lauer, and M. A. Sandau, *Zhurnal Analiticheskoi Khimii*, **25**, (1970) 2118.

17. A. T. Pilipenko and T. L. Shevchenko, *Zhurnal Analiticheskoi Khimii*, **7**, (1989) 1262.

18. J. C. Stockert, A. R. Llorente, P. Del Castillo, and G. Gomez, *Stain Technology*, **65**, (1990) 299.

19. Riboh, M., *Food Engineering*, (1977) 66.

20. A. G. Lloyd, *Food Chemistry*, **5**,(1980) 91.

21. J. Racemis and G. Blanchard, personal communication.

22. Allevi, P. et al., *Journal of the Chemical Society Communications*, (1991) 1319.

23. D. L. Klug, in: Handbook of Industrial Crystallization, Ed. A. S. Myerson (Butterworth-Heinemann, 1993) p. 82.

Chapter Four

Future Work

4.1 Assignment of the fundamental lattice Raman bands for cimetidine crystals

Tudor *et. al* [1] has made tentative assignments for cimetidine in the fingerprint region of the Raman spectrum, but there have been no assignments made of cimetidine in the lattice vibration region. Turrell[2] gives a detailed description, showing how various fundamental lattice vibrations can be attributed to librational motions around the x, y, and z axes.

The first step in determining fundamental lattice vibration assignments would be to obtain the crystalline structure of each respective phase through x-ray crystallography. The crystalline structure of ciimetidine form A has been determined to be $P_{21/c}$ by several authors[3,4,5], but the crystalline structure of form B has not been published. In order to determine the crystalline structure of form B, it would be preferable to grow a form B crystal of suitable size[6] and then determine the lattice parameters. An x-ray powder diffraction could also be done, but x-ray crystallography would be preferred.

Large crystals of form B have proven difficult to grow[7,8], but it appears that the best solvent mix would be approximately 1.75/1 (v/v) isopropanol saturated with respect to form B and undersaturated with respect to form A, where the overall solubility of cimetidine is quite high relative to that in other solvent systems. The high solubility of cimetidine in these solutions provides a better driving force for crystallization, especially for the crystallization of the thermodynamically stable form B. It would be best to seed the fore-mentioned solution with a form B crystals in an unagitated solution, thus reducing secondary nucleation of the stable phase. The optimal temperature of crystallization still needs to be determined, but it appears the higher, the better since solubility increases with increasing temperature. Transformation at higher crystallization temperatures should not be a problem since cimetidine is monotropic with respect to forms A and B.[9]

Once large crystals are grown and the x-ray crystal structure is determined, the fundamental Raman band assignments can be made. For all crystalline structures, there are tables of Raman polarizability tensors calculated[10] which can mathematically predict the polarization of incident and scattered light giving rise to the respective Raman scattering bands. By obtaining Raman spectra of cimetidine at various incident and scattering orientations, the bands can be assigned with respect to unit cell and molecular symmetry. The possibility of Raman spectra arising from multiphonon processes should also be considered, but it would be difficult to actually assign bands since these phenomena have proven to be quite complicated for all but the simplest of molecules.[11]

4.2 Raman spectral investigations of other cimetidine forms

There have been seven different crystalline forms of cimetidine[12] discovered since 1976, with each exhibiting different infrared spectra. From the work of Tudor *et al.*[1], it has been shown that cimetidine exhibits different Raman spectral characteristics in the fingerprint regions between forms A, B, and C, but the spectra of these forms have not been investigated in the lattice vibration region. A more comprehensive understanding of the Raman spectra of the other known forms of cimetidine should be done to complete the basic research done up to this point. This would provide background information which could be used to investigate the possibility of other phase transformations and/or crystallization conditions.

4.3 Cimetidine crystallization experiments

The work done heretofore has shown that phase transformations can be observed using Raman spectroscopy, but crystallization from a seeded, supersaturated solution has yet to be investigated. Sudo *et al.*[8] has used more traditional methods to observe the crystallization of cimetidine under different conditions of seeding, supersaturation, and

temperature, but they have not investigated the effect of different solvents. As mentioned previously, the capability Raman spectroscopy to obtain measurements in situ presents a great potential to determine crystallization parameters with little or no disruption of the system under study. *In situ* Raman spectra of cimetidine slurries can be greatly improved through better instrumentation, which will be discussed below. Once the *in situ* Raman spectroscopy of cimetidine slurries is perfected, the experiments of Sudo et. al should be repeated using Raman spectroscopy *in situ* and the results compared to verify the use of this technique as a plausible substitute for more traditional methods. After this, crystallization experiments should be carried out in at least two solvents other than isopropanol, preferably one with lower cimetidine solubility and one with higher cimetidine solubility. Two logical solvents for these experiments would be water (lower solubility) and water-isopropanol (higher solubility). Several parameters should be investigated. The effect of supersaturation, seed crystal form, agitation rate, and temperature are all variables that can be considered. The possibility of solvent-mediated phase transformations during crystallization experiments should also be examined, especially if a mixture of seed crystal forms is used.

4.4 Improvements in Instrumentation of Raman Spectroscopy

All the Raman spectra have been obtained using a Spex Triplemate 1877 coupled to an EG & G CCD, red-enhanced detector. In the past this instrumental configuration has proven to be quite useful in obtaining high resolution Raman spectra with good Rayleigh line rejection, but the majority of these experiments have been done using blue excitation, where the Raman efficiency is much better than experiments done with visible red or infrared excitation. The triplemate configuration consists of three monochrometers and three dispersion gratings. For each grating, a loss of 50% throughput occurs, thus the signal that actually gets to the detector is reduced significantly by just the gratings alone,

not to mention many of the other optics that are downstream from the sample position. When using visible red excitation, this can greatly diminish the signal to noise ratio since the loss from the gratings is coupled to the ν^4 dependence of Raman scattering on excitation frequency.

Considerable improvements in instrumentation for Raman spectroscopy have potential to greatly improve the signal to noise ratio, thus allowing for higher quality spectra and reduced power needs. The use of holographic notch filters coupled to a single dispersion grating and CCD detector gives throughput up to an order of magnitude higher than that of a triple monochrometer while still attenuating Rayleigh scatter enough to obtain Raman spectra as low as 64 cm^{-1}. Pallister *et al.*[15] has demonstrated the use of this new technology by coupling holographic notch filters and beam splitters to a Raman microprobe, but this equipment could be modified for a conventional macroscopic sample chamber.[14] By using this technology, the beam could be directed to a batch reactor with a crystallizing slurry in a backscattering configuration, allowing for spectra to be detected from both phases during the process. The high throughput would allow for much shorter accumulation times, thus giving data points which would be more accurate as a function of time.

Another possibility is the use of a fiber optic coupled to holographic notch filters and a single dispersion grating. The fiber optic probe could be used as a remote sensing device that could be dipped directly into a crystalline slurry. The use of a configuration similar to this has been demonstrated for the emulsion polymerization of polystyrene.[15] The authors obtained Raman spectra of both the solid phase polystyrene and the liquid phase styrene monomer. They were able to follow the disappearance of the monomer phase and the appearance of the solid polymer as a function of time. These spectra were obtained in the fingerprint region with an excitation of 514.5 nm, but it appears feasible that the experiment could be applied to crystalline slurries using visible red excitation to obtain Raman spectra in the lattice vibration region.

4.5 Carminic Acid

Studies should be undertaken to better understand the potential use of carminic acid as a trace fluorescent probe in aqueous food systems. The work done so far has been limited to studies in sucrose and glucose solutions, thus work needs to be done in other sugars and possibly other food systems to give a more complete picture of carminic acid's use as a trace fluorescent probe.

Experiments are necessary to assign fluorescence bands in both the UV and visible regions to functional groups on the molecule. Similar analysis has been done for other benzyl-anthraquinones,[16,17] but carminic acid has not been characterized. This would involve starting with a molecule of known fluorescence band assignments, such as anthraquinone, and adding functional groups until the carminic acid molecule is completely synthesized. After each functional group addition, the fluorescence spectra could be taken, and the emission bands assigned. In this way, each successive fluorescence band that arises could be accounted for by equating the spectral changes to the newly added functional group. A study such as this would be very challenging since it would involve expertise in both fluorescence spectroscopy and organic chemistry.

Several different protonated and deprotonated species that exhibit different spectra, but a detailed analysis of the fluorescence characteristics should be done to better understand what is happening in the solute-solvent system being probed. Determination of excited state pKa's is necessary to better understand the effects of pH on fluorescence spectra. By using the Forster cycle[18], the excited state pKa's can be calculated with the shift between the absorption and fluorescence peaks. Similar studies have been done on mono and bi-substituted phenols, but these compounds have well resolved fluorescence spectra. The challenge lies in the deconvolution and assignment of the fluorescence bands.

Other FDA approved substances that are chemically similar to carminic acid offer potential as trace fluorescent probes in sugar solutions[19]. Kermesic acid[20] has the same chemical structure as carminic acid except it has a hydrogen group in place of the glucose group. Its violet-red color suggests that visible excitation may result in fluorescence spectra similar to carminic acid. Some of the carmine lakes also show promise as trace fluorescent probes provided that the system under study is free of transition metal ion impurities.

4.6 Crystallization Studies of Carminic Acid Doped sugar solutions

The value of a trace fluorescent probe lies in its ability to monitor system parameters with minimal effects on the system, thus it is important to understand these potential effects. Carminic acid can be used to study the crystallization of sugars *in situ*, but the effect of this probe on crystallization kinetics and the potential for carminic acid to function as a tailor-made impurity should be studied first. The glucose group in carminic acid's structure makes it a tailor-made impurity,[21] which could slow the crystallization kinetics, change the crystal morphology, and increase or decrease the solubility of the sugars in aqueous solution.

By varying the amount of carminic acid in aqueous sugar solutions during crystallization, kinetics, crystal morphology, and inclusion can be studied as a function of probe concentration. These studies should be done in both unagitated and agitated solutions to factor in the effect of secondary nucleation. Seeded and unseeded solutions also need to be looked at. Once carminic acid's effect on aqueous sugar solution crystallization are known, it can be used to study aqueous sugar solution conditions during crystallization by using a probe concentration that minimally affects the system while still allowing for monitorization of the system. Experiments with carminic acid-doped sugar solutions would allow for observation of solution side conditions during crystallization.

An excitation wavelength of 310 nm would give the best results since spectral changes are more pronounced when this excitation is used.

References

1. A. M. Tudor, et. al. *SpectroChimica Acta*, **47A**, (1991) 1389.

2. Infrared and Raman Spectra of Crystals, G. Turrell, (Academic Press, London, 1972), pp. 159-167.

3. B. Prodic-Kojic et. al., *Gazetta Chimica Italiana*, **109**, (1979) 535.

4. M. Shibata, et. al, *Journal of Pharmaceutical Sciences*, **72**, (1983) 1436.

5. E. Häddicke, F. Frickel, and A. Franke, *Chem. Ber.*, **111**, (1978) 3222.

6. J. W. Jeffery Methods in x-ray crystallography (London, New York, Academic Press, 1971) pp. 1-3.

7. B. Hegedüs and S. Görög, *Journal of Pharmaceutical and Biomedical Analysis*, **3**, (1985) 303,.

8. S. Sudo, K. Soto, and Y. Harano, *Journal of Chemical Engineering of Japan*, **24**, (1991) 237.

9. S. Sudo, et. al., *Memoirs of the Faculty of Engineering, Osaka City University* , **31**, (1990) 61-67.

10. W. G. Fateley, et. al. Infrared and Raman Selection Rules for Molecular and Lattice Vibrations, (Wiley Interscience, New York, 1972) Appendix I and II.

11. G. Turrell, Infrared and Raman Spectra of Crystals, (Academic Press, New York, 1972) Chapter 5 and 6.

12. British Patent Specification, No. 1543238 (1976)

13. D. M. Pallister, et. al., *Applied Spectroscopy*, **46**, 1469 (1992).

14. Kaiser Optical Product Literature, January 1995.

15. C. Wang, T. J. Vickers, J. B. Schlenoff, and C. K. Mann, *Applied Spectroscopy*, **46**,(1992) 1729.

16. N. V. Platonova, K. R. Popov, and L. V. Smirnov, *Optical Spectroscopy*, **34**, (1969) 197.

17. D. K. Palitm, T. Mukherjee, and J. P. Mittal, *Journal of the Indian Chemical Society*, **63**, (1986) 35.

18. E. L. Wehry, and L. B. Rogers, *Journal of the American Chemical Society*, **87**, (1965) 4234.

19. D. D. Gadgil, A. V. Rama Rao, and K. Venkataraman, *Tetrahedron Letters*, **18**, (1968) 2223.

20. O. Dimroth, *Berichte der Deutschen Chemichen Gesellschaft*, **43**, (1910) 1387.

21. S. N. Black, R. J. Davey, and M. Halcrow, *Journal of Crystal Growth*, **79**, (1986) 765.

APPENDIX

Original Data from Scatter Plots

APPENDIX

Original Data from Scatter Plots

Table III: Original Data from Figure 12

Wt % Cim	PIR(675 cm-1/494 cm-1)	
0.00	0.0013	solubility A: Weight %=4.96, PIR=0.289
1.00	0.0630	solubility B: Weight %=3.77, PIR=0.217
2.00	0.128	
3.00	0.175	
4.00	0.242	
5.00	0.294	
6.00	0.378	

Table IV: Original Data from Figure 13

Wt % Cim	PIR(675 cm-1/494 cm-1)	
0.00	0.00	solubility A: Weight %=14.2, PIR=0.1.69
2.50	0.329	solubility B: Weight %=10.8, PIR=0.1.39
5.00	0.600	
7.50	0.955	
10.0	1.24	
12.5	1.59	
15.0	2.02	

Table V: Original Data from Figure 15 (All PIR's 675 cm-1/494 cm-1)

Time (hours)	PIR 0% B initial	PIR 25% B initial	PIR 50% B initial	PIR 75% B initial	PIR 100% B
0.00	0.306	0.314	0.314	0.304	0.314
4.00	0.315	0.300	0.300	0.298	0.294
10.0	0.306	0.304	0.294	0.310	0.275
20.0	0.310	0.298	0.304	0.276	0.254
28.0	0.304	0.306	0.308	0.258	0.252
36.0	0.298	0.302	0.310	0.254	0.248

Table VI: Original Data from Figure 16 (All PIR's 675 cm-1/494 cm-1)

Time (hrs)	PIR 0% B initial	PIR 1% B initial	PIR 25% B initial	PIR 50% B initial	PIR 75% B initial	PIR 100% B
0.00	1.90	1.87	1.87	1.83	1.89	1.86
0.500	1.85	1.84	1.85	1.84	1.84	1.83
1.00	1.87	1.89	1.84	1.78	1.81	1.79
2.00	1.83	1.83	1.75	1.71	1.69	1.65
3.00	1.81	1.81	1.63	1.65	1.63	1.60
6.00	1.83	1.85	1.54	1.56	1.57	1.55
10.0	1.85	1.83	1.49	1.51	1.50	1.50
16.0	1.84	1.63	1.49	1.48	1.49	1.45
24.0	1.89	1.49	1.47	1.46	1.48	1.45

Table VII: Original Data from Figure 24

Wt % Glucose	PIR (594 nm/610 nm)
30.0	0.949
40.0	0.948
50.0	0.973
60.0	0.994
65.0	1.036
70.0	1.062
75.0	1.116
80.0	1.167

Table VIII: Original Data from Figure 25

Wt % Glucose	PIR (594 nm/450 nm)
20.0	4.10
30.0	5.08
40.0	5.98
50.0	7.16
60.0	9.75
70.0	12.1
80.0	14.9

Table IX: Original Data from Figure 26

Wt % Glucose	pH
30.0	6.35
40.0	5.95
50.0	5.45
60.0	5.05
65.0	4.90
70.0	4.65
75.0	4.38

Table X: Original Data from Figure 27

Wt % Glucose	PIR (594 nm/610 nm)	Buffer pH	PIR (594 nm/610 nm)
30.0	0.949	6.20	0.964
40.0	0.948	5.75	0.961
50.0	0.973	4.90	0.970
60.0	0.994	4.35	0.950
65.0	1.036		
70.0	1.062		
80.0	1.167		

Table XI: Original Data from Figure 28

Wt % Glucose	PIR (594 nm/450 nm)	Buffer pH	PIR (594 nm/450 nm)
20.0	4.10	6.50	0.711
30.0	5.08	5.67	0.547
40.0	5.98	4.15	0.542
50.0	7.16		
60.0	9.75		
70.0	12.1		
80.0	14.9		

Table XII: Original Data from Figure 31

Wt % Sucrose	PIR (610 nm/580 nm)
20.0	1.12
30.0	1.11
40.0	1.11
50.0	1.12
60.0	1.14
70.0	1.12
75.0	1.11

Table XIII: Original Data from Figure 32

Wt % Sucrose	PIR (594 nm/450 nm)
20.0	0.750
30.0	0.390
40.0	0.438
50.0	0.868
60.0	1.70
70.0	4.28
75.0	7.20

Table XIV: Original Data from Figure 33

Wt % sucrose	pH
20.0	8.65
30.0	8.35
40.0	8.03
50.0	7.75
60.0	7.35
70.0	6.95
75.0	6.51

Table XV: Original Data from Figure 34

Wt % Sucrose	PIR (610 nm/580 nm)	Buffer pH	PIR (610 nm/580 nm)
20.0	1.12	8.75	1.03
30.0	1.11	8.14	1.05
40.0	1.11	7.75	1.09
50.0	1.12	7.50	1.07
60.0	1.14	6.96	1.06
70.0	1.12		
75.0	1.11		

Table XVI: Original Data from Figure 35

Wt % Sucrose	PIR (594 nm/450 nm)	Buffer pH	PIR (610 nm/580 nm)
20.0	0.750	8.30	0.671
30.0	0.390	7.74	0.847
40.0	0.438	6.50	0.875
50.0	0.868		
60.0	1.70		
70.0	4.28		
75.0	7.20		